Organic, gas, and element geochemistry of hydrothermal fluids of the newly discovered extensive hydrothermal area in the Wallis and Futuna Region (SW Pacific)

C. Konn, J. P. Donval, V. Guyader, E. Roussel, E. Fourré, P. Jean-Baptiste, E. Pelleter, J. L. Charlou, Y. Fouquet

Hindawi
Geofluids
Volume 2018, Article ID 7692839, 25 pages
https://doi.org/10.1155/2018/7692839

Research Article

Organic, Gas, and Element Geochemistry of Hydrothermal Fluids of the Newly Discovered Extensive Hydrothermal Area in the Wallis and Futuna Region (SW Pacific)

C. Konn,[1] **J. P. Donval**,[1] **V. Guyader**,[1] **E. Roussel**,[2] **E. Fourré**,[3] **P. Jean-Baptiste**,[3] **E. Pelleter**,[1] **J. L. Charlou**,[1] **and Y. Fouquet**[1]

[1]*Ifremer, Laboratoire des Cycles Géochimiques et Ressources, CS10070, 29280 Plouzané, France*
[2]*Ifremer, Laboratoire de Microbiologie des Environnements Extrêmes, CS10070, 29280 Plouzané, France*
[3]*LSCE, UMR 8212 CEA-CNRS-UVSQ, 91191 Gif-sur-Yvette, France*

Correspondence should be addressed to C. Konn; cecile.konn@ifremer.fr

Received 23 June 2017; Revised 31 October 2017; Accepted 17 December 2017; Published 11 March 2018

Academic Editor: Xing Ding

Two newly discovered hydrothermal vent fields of the Wallis and Futuna region, Kulo Lasi and Fatu Kapa, were sampled for fluid geochemistry. A great geochemical diversity was observed and assigned to the diversity of lithologies as well as the occurrence of various processes. Kulo Lasi fluids likely formed by interaction with fresh volcanic rocks, phase separation, and mixing with magmatic fluid. Conversely, the geochemistry of the Fatu Kapa fluids would be mostly due to water/felsic lavas reactions. In terms of organic geochemistry, fluids from both fields were found to be enriched in formate, acetate, and semivolatile organic compounds (SVOCs): n-alkanes, n-fatty acids, and polyaromatic hydrocarbons (PAHs). Concentrations of SVOCs reached a few ppb at most. The distribution patterns of SVOCs indicated that several processes and sources, at once of biogenic, thermogenic, and abiogenic types, likely controlled organic geochemistry. Although the contribution of each process remains unknown, the mere presence of organics at the μM level has strong implications for metal dispersion (cycles), deposition (ore-forming), and bioavailability (ecosystems), especially as our fluxes estimations suggest that back-arc hosted vent fields could contribute as much as MOR to the global ocean heat and mass budget.

1. Introduction

Although back-arc settings are favourable environments for the formation of hydrothermal convection cells, hydrothermal exploration has long been conducted to a greater extent on Mid-Oceanic Ridges (MOR). Today, more than 600 active hydrothermal vent fields have been discovered and about half of them are located at MOR against a fifth in back-arc basins (BAB) [1]. Yet back-arc environments are likely to generate more diversity than their MOR homologs in terms of fluid chemistry because of the variety of lithologies the fluids can react with (e.g., basaltic to rhyolitic volcanic rocks with or without arc-like geochemical signature, various alteration mineralogical assemblages) as well as the possible contribution of magmatic-related aqueous fluids [2–5]. The Wallis and Futuna area was surveyed for hydrothermal activity because of its very peculiar geological settings within a back-arc system and its potential relevance for mineral resources [6, 7]. It is located about 200 km west of the northern tip of the Tonga-Kermadec trench where the fastest subduction rates have been recorded (18 to 24 cm per year) and occur at the junction of 2 BAB: the Lau and the North-Fiji BAB [8]. Here we report on the geochemistry of the fluids of the very first two vent fields discovered in the area and in this type of environment. We chose to bring a special focus on organic geochemistry because it has been hardly studied in modern hydrothermal systems despite the recent growing interest for organic matter (OM) in the ocean. The discussion focuses on processes controlling the geochemistry as well as implications of the presence of organic molecules at the local and regional scales.

Organic geochemistry of hydrothermal fluids has generally been far less studied than the mineral and gas geochemistry. In most cases works focused on small molecules (hydrocarbon gases, volatile fatty acids, and amino acids) and very few data are available on semivolatile organic compounds (SVOCs). Despite the growing interest for OM in the ocean and hydrothermal systems there is still a major lack in identification and quantification of organic compounds [10–15]. Notably numbers of studies agree on the major ligand role of organics in metal stabilisation, transportation, bioavailability, and ore-forming but there are hardly any clues on the nature of these ligands in hydrothermal environments [16–25]. Organic compounds in hydrothermal fluids may come from marine dissolved organic matter (DOM) recycling [12, 13], subsurface biomass degradation [26], entrainment of organic detritus from local recharge zones, and subsequent degradation, or abiotic formation in the deep subsurface [27–30]. The latter is supported by many theoretical [31–33] and experimental work summarised in two reviews [34, 35]. Conversely, some other studies reported the absence of organic compounds in hydrothermal fluids except at the Lost City alkaline vent field which is theoretically more favourable for abiotic synthesis [36]. Nevertheless, we report here the presence of semivolatile organic compounds in hydrothermal fluids from the Wallis and Futuna area and provide concentrations of a selection of extractable compounds that have been identified elsewhere as hydrothermally derived [27, 37]: n-alkanes, n-fatty acids (n-FAs), mono-, and polyaromatic hydrocarbons (BTEXs and PAHs). These very first quantitative field data might feed thermodynamic models of abiotic synthesis, guide the design of experiments to better understand hydrothermal organic geochemistry, and help assessing the importance of hydrothermally derived organic compounds in metal complexation and, as a nutrient for microorganisms, complete fluxes calculation and enter in the carbon cycle budget calculations.

2. Geological Settings

Wallis and Futuna Islands are located at the transition between the North Fiji and the Lau back-arc basins. This geodynamical setting accounts for complex volcanic and tectonic activity in the area. Pelletier et al. [38] and Fouquet et al. [6] observed multiple active extensional zones including widespread areas composed of numerous individual volcanoes (e.g., Southeast Futuna volcanic zone (SEVZ)) and well organised spreading centers such as the Futuna and Alofi oceanic ridge. West of Futuna Island, the 20–30° trending Futuna spreading center (FSC), is composed of a series of en echelon spreading segments. The opening rate of this oceanic ridge has been estimated at 4 cm/yr from the interpretation of magnetic anomalies [38]. East and southeast of Futuna Island, bathymetric maps, and reflectivity data clearly reveal that active extension and recent volcanism occur in the SEVZ as well as along the Alofi spreading center [6]. The SEVZ is a broad zone of diffuse volcanism bordered by the ENE-WSW trending volcanic graben (named Tasi Tulo graben) to the north and the NNE-SSW trending Alofi spreading center to the south. The SEVZ includes Kulo Lasi active volcano, the Fatu Kapa, and Tasi Tulo volcanic zones ([7], Figure 1).

Fluids were sampled at the Kulo Lasi and Fatu Kapa sites. Kulo Lasi has been described in detail by Fouquet and collaborators [39]. In summary, it is a shield volcano located about 100 km southeast of Futuna Island (Figure 1). It represents the most recent volcano in the SEVZ and is composed of basaltic to trachy-andesitic lava with no direct geochemical affinity with subduction [39]. The volcanic edifice is ca. 20 km in diameter and appears relatively flat with the top located at a depth of 1200 m and the base only 300 m deeper (ca. 1500 m below sea level). It exhibits a central caldera (5 km in diameter and 200–300 m deep) with a flat bottom covered by recent lavas and a central mound composed of older and tectonised lava flow. By contrast, the Fatu Kapa volcanic area is in a 20 km wide transition zone between the Tasi Tulo graben and the Kulo Lasi volcano. Here only small (<1 km) volcanic edifices are seen to be consisting of young mafic to felsic lavas (Figure 1).

3. Sampling and Analytical Procedures

Sampling was achieved at Kulo Lasi and Fatu Kapa by the HOV Nautile during the FUTUNA 1 and FUTUNA 3 cruises conducted by Ifremer in 2010 and 2012. Fluid samples were taken at the nose of smokers to minimise seawater contamination. Samples of volumes up to 750 mL of hydrothermal fluids were collected in titanium syringes that were modified after the model described in Von Damm et al. [40]. The gas-tightness was greatly improved and ensured the majority of the gas to be recovered. Those same syringes have been used in several studies by Charlou et al. and have shown good results notably for gas-Mg correlations (e.g., Charlou et al., 2002). Autonomous temperature sensors (*S2T 6000-DH, NKE Instrumentation*) were mounted on the sampler nozzle. As soon as the fluids were recovered, pH, H_2S, and Cl^- concentrations were measured to evaluate the quality of the sample. Total gases were immediately extracted and analysed; then aliquots of gas were conditioned for further stable isotopes measurements. Finally, the gas-free fluid was conditioned for major and minor elements analyses, on the one hand, and for organic compounds analyses, on the other hand.

3.1. Gas Extraction and Analyses. Total gas was extracted as described in Charlou and Donval [41]. Preliminary major gases (CO_2, H_2, CH_4, and N_2) concentrations were obtained on board by using a portable chromatograph *(Microsensor Technology Instruments Inc.)* that was mounted on line with the gas extractor. Extracted gases were conditioned on board in stainless steel pressure-tight flasks and stored until analyses. Gases were separated by Gas-Chromatography (Agilent GC 7890A, *Agilent Technologies*) and quantitatively analysed by triple detection using mass (MS 5975C, *Agilent technologies*), flame ionisation, and thermal conductivity detectors. Aliquots of gas were stored both in vacuum tight tubes *(Labco, Ltd.)* and in copper tubes to be sent for further carbon isotope analyses *(Isolab b.v., Netherlands)* and He isotopes analyses *(CEA, Saclay, France)*, respectively.

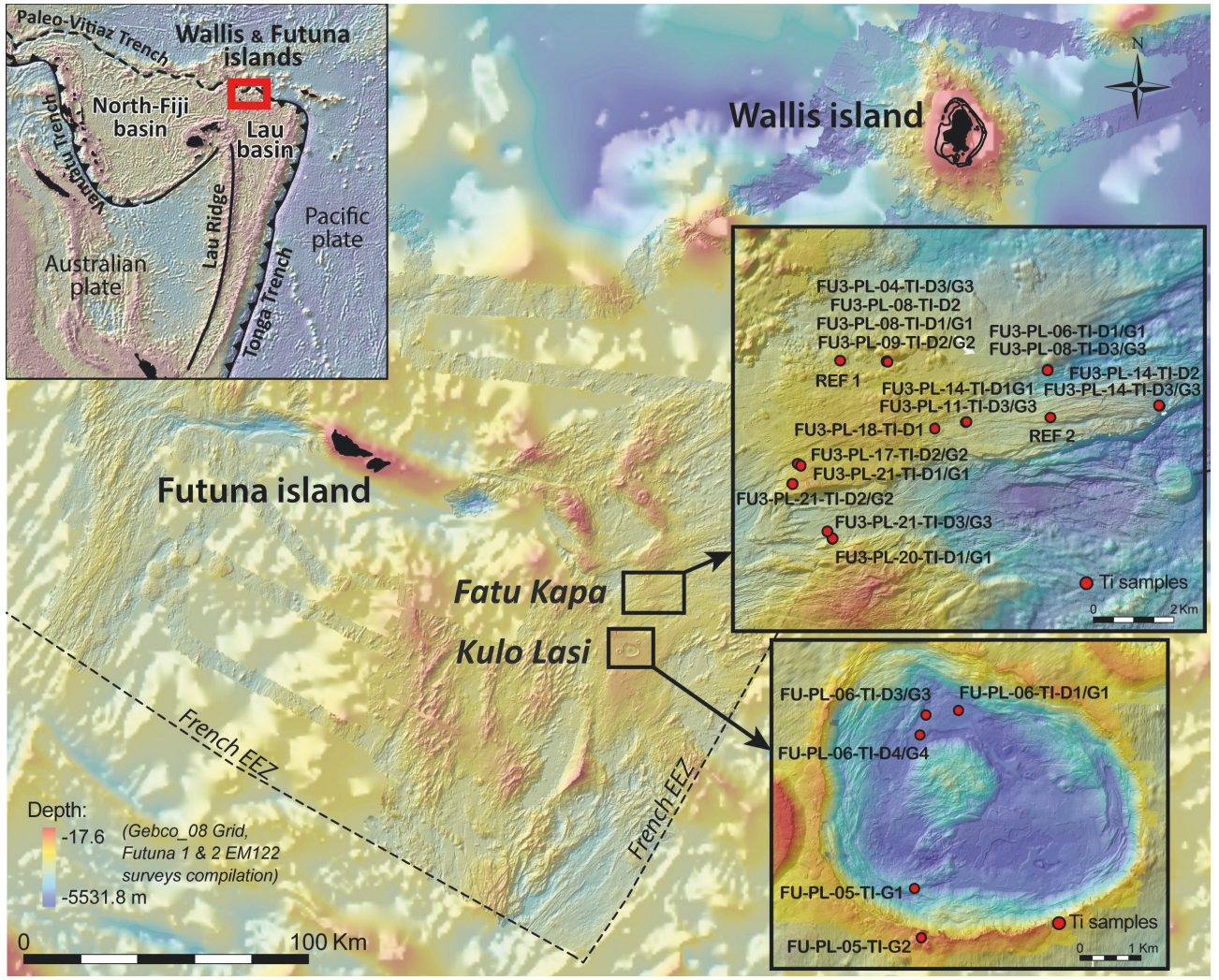

Figure 1: Bathymetric map of the study area. Close-ups of Fatu Kapa and Kulo Lasi are shown in boxes where sample positions are marked with red disks. Copyrights from Ifremer, FUTUNA 1, 2, and 3 cruises.

3.2. Inorganic Geochemistry: Sample Preparation and Analyses. pH was measured using a combined glass electrode *(Ecotrode Plus, Metrohm)*. Cl^- and H_2S were measured by potentiometry using $AgNO_3$ (0.05 M) and $HgCl_2$ (0.01 M) as titrating solutions, respectively. NaOH (2 M) was added to the aliquot before H_2S measurement. SO_4, Br, Na, K, Mg, Ca, Li, and Cl were measured by ionic chromatography *(Dionex Ion Chromatograph System 2000)* after appropriate dilutions. Fe, Mn, Cu, Zn, Sr, Li, and Rb were measured by flame atomic absorption spectrometry using standard additions *(AAnalyst, Perkin Elmer Inc.)*. Aliquots for silica determination were immediately diluted 100- to 200-fold and analysed by the silicomolybdate automatic colorimetric method [42, 43].

3.3. Organic Geochemistry. Total Organic Carbon (TOC) was measured using a multi N/C 3100 *(Analytik Jena AG, Germany)*. Samples were acidified online with HCl and then purged with O_2 to remove inorganic carbon (IC). A TIC control analysis was performed and followed by three TOC measurements on each sample.

Acetate and formate concentrations were determined using a Dionex ICS-2000 Reagent-Free Ion Chromatography System equipped with an AS50 autosampler *(Dionex Camberley, UK)*. Chromatographic separation was conducted using two Ionpac AS15 columns in series at 30°C and the determination of species was carried out using an Anion Self-Regenerating Suppressor *(ASRS 300 4 mm)* unit in combination with a DS6 heated conductivity cell (35°C). The gradient program was as follows: 6 mmol L^{-1} KOH (43 min); increase from 27 mmol L^{-1} KOH min^{-1} to 60 mmol L^{-1} (39 min); decrease from 54 mmol L^{-1} KOH min^{-1} to 6 mmol L^{-1} (5 min).

SVOCs were extracted using Stir Bar Sorptive Extraction (SBSE). Basically any compound with a log Ko/w > 2.5 is recovered with a rate > 50% [44]. The method was improved after Konn et al. [37]. The entire content of the titanium

Table 1: Main GC analytical parameters used for calibration and analyses of hydrothermal fluid samples. Each group of compounds (n-alkanes, BTEXs, PAHs, and n-fatty acids) was analysed using separate twisters.

	n-Alkanes	BTEX & PAHs	n-Fatty acids
Oven			
Initial T (°C)	40	40	40
Initial t (min)	1	1	1
ramp	40 to 320°C at 12°C/min	40 to 320°C at 12°C/min	40 to 320°C at 20°C/min
Final T (°C)	320	320	320
Final t (min)	2	2	2
Injector			
T (°C)	250	250	325

Table 2: Experimental conditions used for calibration curves. Linear regressions were performed on one order of magnitude concentration domain depending on the concentration range of the samples.

	n-Alkanes	BTEX & PAHs	n-Fatty acids
Concentration levels ($\mu g \cdot L^{-1}$)	0.5, 1, 2, 5, 10	0.05, 0.1, 0.25, 0.5, 1, 2, 5, 10	0.25, 0.5, 1, 2, 5, 10
IS concentration ($\mu g \cdot L^{-1}$)	5	5	10

syringe was transferred into a precombusted glass bottle and six 90 mL aliquots of the sample were poured into 100 mL precombusted glass vials. 10 mL of MeOH was added to avoid adsorption of the compounds onto the wall of the vials. Internal standards were added to the solutions in 2012 so that quantification could only be achieved in Fatu Kapa fluids. Extraction was performed in sealed vials with ultrainert septum crimps, at 300 rpm and using 48 μL PDMS Twisters® (*Gerstel GmbH*). We focused on a selection of chemical groups that had previously been described as hydrothermally derived [27]. To that respect, pairs of aliquots were dedicated to analysis of n-alkanes, n-FAs, and both BTEXs and PAHs, respectively. Extraction kinetics experiments showed that chemical equilibrium was reached after 5 h of extraction for n-alkanes, 4 h for PAHs and 14 h for n-FAs (Konn, unpublished results). Twisters were then removed, rinsed with MQ water, dried, and stored at +4°C until analyses by Thermal Desorption-Gas Chromatography-Mass Spectrometry (TD-GC-MS) [37]. Analytical parameters were adjusted for each group of compounds (Table 1).

For each batch of conditioned Twisters, one was spared, stored at +4°C, and analysed in the same run as the other Twisters. This dry blank aimed at showing any contamination that could have occurred during conditioning, storage, and transport. MQ water samples were prepared and extracted on board as regular hydrothermal samples to check if any contaminations could have occurred during the sample preparation step. Deep-sea water was also collected, processed, and analysed, using the same titanium syringes and according to the same protocols as for hydrothermal fluid samples, and thus constitute the reference blank experiment.

Calibration was achieved using a commercial standard solution of BTEXs and 3 custom standard solutions of C_9–C_{20} n-alkanes, C_6–C_{18} n-FAs, and PAHs containing naphthalene (N), Acenaphtene (A), Fluorene (F), Phenanthrene (Ph), Anthracene (An), Fluoranthene (Fl), and pyrene (Py) *(LGC Standards, LGC Ltd.)*. Deuterated n-alkanes ($C_{10}D_{22}$ and $C_{14}D_{34}$), methyl esters ($C_9H_{18}O_2$ and $C_{15}H_{30}O_2$), and deuterated PAHs (naphthalene-D8, Biphenyl-D8, and Phenanthrene-D10) were used as internal standards (IS). Calibration curves (Concentration (analyte)/Concentration (IS) versus Area (analyte)/Area (IS)) were obtained using at least five concentration levels that were replicated 3 times (Table 2). Although the correlation coefficient of the linear regressions was satisfactory for all compounds, the significance and lack of fit of the model were checked by statistical tests before validation. A series of Student, Barlett, Chi-square, and Fisher tests was run for each individual compound using the Lumière software. The best fitting model was then chosen for each case and confidence intervals were calculated.

4. Results

Altogether 35 hot fluid samples were collected in the study area from 8 different sites: Kulo Lasi caldera (6), on the one hand, and Stéphanie (7), Carla (4), Idef^X (4), Obel^X (3), Aster^X (1), Fati Ufu (6), and Tutafi (4), on the other hand, all located in the Fatu Kapa area (Figure 1). The Kulo Lasi smokers occurred at ~1500 m depth on recent lava flows and consisted in a multitude of short (~25 cm) and narrow (~3–5 cm) diameter anhydrite chimneys containing a small percentage of sphalerite (ZnS), chalcopyrite ($CuFeS_2$), isocubanite ($CuFe_2S_3$), pyrrhotite ($Fe_{1-x}S$), and pyrite (FeS_2) (Figure 2). The temperature was consistently about 343°C and the pH approached 2.2–2.3 (Table 3). In the Fatu Kapa area we could distinguish two types of hydrothermal environments at 1550–1650 m depth. Translucent 270–290°C fluids associated with anhydrite chimneys (up to 25 m tall and 2.5 m in diameter) characterised Stéphanie, Carla, Idef^X, Obel^X, and Aster^X sites, while >300°C milky to grey fluids associated with sulphide chimneys were characteristic of the southwest region including Fati Ufu and Tutafi sites (Figure 3, Table 3).

4.1. Gas. Concentrations of gases in all fluids as well as stable isotopes data are compiled in Table 4. Samples recovered

Figure 2: Photographs of sulphide chimneys and young lava flows observed on the floor of the Kulo Lasi caldera. Copyrights from Ifremer, FUTUNA 1 cruise.

from Kulo Lasi were extremely poor in CH_4 (<0.01 mM) but contained the series of C_2–C_5 hydrocarbons. Samples from Fatu Kapa had higher concentration of CH_4 (0.05–0.235 mM) but only n-pentane (0.5–3.2 μM) could be detected and quantified in terms of longer hydrocarbons. One sample from Kulo Lasi was found to be extremely rich in H_2 with nearly 20 mM while the others ranged from 1 to 6 mM and were below 0.05 mM at Fatu Kapa. H_2S was highly variable between the 3 sampled chimneys at Kulo Lasi (0.39, 1.66, and 5.05 mM) while it was found rather homogeneous at Fatu Kapa with values around 1 mM. CO_2 concentrations were more elevated at Fatu Kapa (4.5–29 mM) compared to Kulo Lasi (1–5 mM).

Helium isotope ratios were in the range 7.0–9.9 Ra over the Fatu Kapa area, in agreement with plume data [7]. They could not be measured at Kulo Lasi unfortunately. Carbon isotopes ratios were around −5‰ for CO_2 at Fatu Kapa whereas at Kulo Lasi the ratio showed very different results ranging from −0.2 to −4.1‰. As for methane, $\delta^{13}C$ were slightly lower at Kulo Lasi (~−28‰) versus Fatu Kapa (~ −23‰) and δD was about −110‰ in all samples from Fatu Kapa. δD (CH_4) could not be measured in the Kulo Lasi fluids because of the too low concentrations of CH_4. Carbon isotope ratios of longer hydrocarbons were in the −27 to −22‰ at both vent fields. To be noted one sample from Fati Ufu in the Fatu Kapa area showed remarkably lower isotopic ratios with $\delta^{13}C$ (CO_2) = −2.3‰, $\delta^{13}C$ (CH_4) = −6.1‰ and δD (CH_4) = −93‰. We do not have any explanation for this but do not have any reasons either to consider it as an outlier.

4.2. Major and Minor Elements. Major and minor elements measurements data are compiled in Table 3. Fluids from Fatu Kapa all exhibited a higher salinity than seawater up to 4.6 wt% NaCl whereas at Kulo Lasi fluids with both lower (2.8 wt% NaCl) and higher (4.3 wt% NaCl) salinity were sampled. Mg and SO_4 concentrations tend to be zero in the purest samples at Fatu Kapa. But, the purest fluids from Kulo Lasi showed significant levels of Mg and SO_4, associated with an extremely acidic pH (<2.5) and a high T (343°C). Although we cannot totally discard that some mixing with seawater occurred, endmember concentrations of the Kulo Lasi fluids were then estimated to be close to the purest fluids sampled whereas they were obtained from mixing lines at Fatu Kapa assuming Mg zero (Table 5).

Fluids from Fatu Kapa were enriched compared to seawater in alkali, alkaline Earth, and transition metals as well as in strontium, bromide, and silica. Conversely, the fluids from Kulo Lasi exhibited a much more complex pattern. They were all highly enriched in transition metals and silica compared to seawater and fluids from Fatu Kapa (e.g., Fe up to ~10 mM). The enrichment versus seawater in alkali metals was not as striking as for Fatu Kapa fluids. As for the alkaline Earth metals, the amount of Ca was identical to seawater and fluids were depleted in Sr compared to seawater. Finally, both depletion and enrichment in Br were observed in the fluids from Kulo Lasi.

4.3. Organic Geochemistry. First of all, we would like to mention that because solubility of organic compounds decreases with T and because samples were processed at room temperature, the measured concentrations are probably lower than in situ concentrations. Moreover, it is very likely that a portion of the OM was adsorbed on small particles in the fluids which are not taken into account using our extraction and analytical techniques. As a result, the concentrations we report here probably represent lower estimates of in situ concentrations. However, since in situ measurement techniques are not available yet, these values are the best estimates we can obtain. Note that they also are the first to be published for SVOCs.

Formate and acetate reached 16.3 and 15.5 μM, respectively, and covaried with Mg in the Kulo Lasi fluids (Figure 4). Concentrations of formate and acetate were significantly higher in the Fatu Kapa area but no correlation with Mg could be observed. Nevertheless, the purest fluids usually showed the highest concentrations. Formate reached 68 ppb at Stéphanie and 722 ppb at Fati Ufu whereas it could not be detected at Idef^X and Tutafi and was not measured at

Table 3: Measured concentration of major and minor elements in hydrothermal fluids from the Kulo Lasi and Fatu Kapa vent fields. FUX-PLYY-TiDZ and FUX-PLYY-TiGZ are replicate samples taken in the same orifice, one after the other, but using 2 individual Ti syringes. *T*max (chimney) is the maximum *T* of the discharged fluid for the given chimney which was recorded by the *T* probe of the submarine before sampling. *T*max (sample) is the maximum *T* of the fluid entering the sampler recorded during sampling by the autonomous sensor that was coupled at the nozzle of the sampler.

Sample name	Zone	Site	Description	Depth	*T*max (sample) °C	*T*max (chimney) °C	pH	d^{20} Kg m^{-3}	S ‰	NaCl (wt%)	Cl mM	Si mM	SO_4 mM	Br μM	Na mM	K mM	Mg mM	Ca mM	Li μM	Li μM	Rb μM	Sr μM	Fe μM	Mn μM	Cu μM	Zn μM	Na/Cl	Br/Cl $\times 10^3$	Na/K	CH_4/Mn
IAPSO	-	-	Standard water	-	-	-	-	-	35	3.2	546	0.0	28.2	839	468	10.2	53.2	10.3	27	27	1.3	90	<LOD	<LOD	<LOD	<LOD	0.9	1.5	46	-
FU-PL-05-TiG2	Kulo Lasi	South (out)	Reference water	1150	-	-	-	1.023	35	3.2	551	0.1	29.0	833	457	9.8	53.2	10.6	25	28	4.4	93	<LOD	<LOD	<LOD	<LOD	0.83	1.5	47	-
FU-PL-05-TiG1	Kulo Lasi	South (in)	Diffuse fluid above worms	1414	32.8	-	5.96	1.023	35	3.2	549	0.2	29.3	833	457	9.9	53.2	10.6	28	52	4.6	92	<LOD	<LOD	1.4	1.5	0.83	1.5	46	-
FU-PL-06-TiG4	Kulo Lasi	North (in)	Beehive type black smoker	1475	134.1	332	6.07	1.022	33	3.0	516	1.0	27.0	822	448	10.6	49.8	10.5	33	54	5.3	84	123	32	1.7	3.1	0.87	1.6	42	-
FU-PL-06-TiD4	Kulo Lasi	North (in)	Beehive type black smoker	1475	136	332	5.58	1.021	31	2.8	485	2.1	23.9	994	406	9.5	45.7	10.2	32	55	6.1	74	78	76	1.3	1.5	0.84	2.0	43	0.010
FU-PL-06-TiG3	Kulo Lasi	North (in)	Translucent smoker	1475	342.3	330.7	2.24	1.017	32	2.9	497	8.2	8.8	738	388	18.5	24.6	11.6	149	156	26	7.3	4796	862	14	45	0.78	1.5	21	0.007
FU-PL-06-TiD3	Kulo Lasi	North (in)	Translucent smoker	1475	337.7	330.7	2.37	1.018	33	3.0	517	8.4	10.7	770	405	16.6	28.6	10.8	115	149	24	9.4	4283	788	4.2	41	0.78	1.5	24	-
FU-PL-06-TiD1	Kulo Lasi	North (in)	Black smoker	1475	343.2	345.1	2.36	1.02	47	4.3	735	14.6	6.2	1135	612	29.5	26.5	10.9	238	249	46	3.4	9884	1416	2.5	175	0.83	1.5	21	-
FU-PL-06-TiG1	Kulo Lasi	North (in)	Black smoker	1475	343.2	345.1	3.32	1.028	44	4.0	689	10.8	12.0	1051	565	23.7	34.9	10.8	176	197	36	9.1	6845	1064	20	77	0.82	1.5	24	0.001
FU3-PL-03-TiD3	Fatu Kapa	20 masf	Reference water	1488	-	-	-	-	-	3.3	565	0.0	28.8	841	483	10.4	54.5	10.7	22	51	6	<LOD	<LOD	<LOD	<LOD	<LOD	0.85	1.5	46	-
FU3-PL-14-TiG2	Fatu Kapa	23 masf	Reference water	1572	2	-	-	-	36	3.3	557	0.0	28.7	841	477	10.4	54.2	10.8	23	nm	nm	nm	nm	nm	nm	nm	0.86	1.5	46	-
FU3-PL-04-TiD3	Fatu Kapa	Stéphanie	Translucent smoker	1554	213	279	4.65	1.03	45	4.1	704	0.7	10.9	1300	519	39.8	18.7	69.6	472	568	80	<LOD	169	166	nm	<LOD	0.74	1.8	13	-
FU3-PL-04-TiG3	Fatu Kapa	Stéphanie	Translucent smoker	1554	213	279	4.64	1.03	44	4.0	686	1.0	12.9	1240	513	36.5	22.5	62.8	420	504	71	169	nm	141	8.2	<LOD	0.75	1.8	14	0.805
FU3-PL-08-TiD1	Fatu Kapa	Stéphanie	Translucent smoker	1555	289	280	4	1.031	49	4.5	770	3.8	1.3	1574	535	54.2	0.8	98.9	705	804	121	268	655	265	6.6	<LOD	0.69	2.0	10	0.886
FU3-PL-08-TiG1	Fatu Kapa	Stéphanie	Translucent smoker	1555	289	280	3.41	1.031	49	4.5	772	4.7	0.7	1592	537	54.7	0.5	98.7	708	807	122	283	167	269	nm	<LOD	0.70	2.1	10	0.762
FU3-PL-08-TiD2	Fatu Kapa	Stéphanie	Translucent smoker	1555	291	280	3.83	1.031	48	4.4	748	4.3	0.5	1537	520	52.9	0.6	95.3	684	806	116	<LOD	148	259	nm	<LOD	0.70	2.1	10	-
FU3-PL-09-TiD2	Fatu Kapa	Stéphanie	Beehive type black smoker + bacterial mat	1650	197	236	5.19	1.026	40	3.7	629	1.7	19.8	1052	500	24.4	37.4	37.8	230	293	36	149	nm	65	nm	1.0	0.79	1.7	21	0.902
FU3-PL-09-TiG2	Fatu Kapa	Stéphanie	Beehive type black smoker + bacterial mat	1559	197	236	5.42	1.025	38	3.5	600	1.0	23.8	959	489	18.5	44.3	26.4	143	193	23	<LOD	nm	23	nm	<LOD	0.81	1.6	26	-
FU3-PL-06-TiD1	Fatu Kapa	Carla	Translucent smoker	1663	278	270	5.03	1.024	37	3.4	576	1.7	18.5	927	482	28.5	35.2	17.9	260	310	42	101	nm	nm	nm	<LOD	0.84	1.6	17	-
FU3-PL-06-TiG1	Fatu Kapa	Carla	Translucent smoker	1663	278	270	4.91	1.024	37	3.4	579	0.7	12.7	984	476	37.8	23.6	22.2	391	455	63	<LOD	18	32	nm	<LOD	0.82	1.7	13	-
FU3-PL-08-TiD3	Fatu Kapa	Carla	Translucent smoker	1664	281	281	2.78	1.024	38	3.5	594	4.5	1.1	1139	479	59.6	0.4	31.5	690	746	104	115	nm	48	nm	4.4	0.80	1.9	8	1.365
FU3-PL-08-TiG3	Fatu Kapa	Carla	Translucent smoker	1664	281	281	4.17	1.024	38	3.5	592	4.0	1.9	1120	477	57.7	2.7	30.3	655	720	96	<LOD	288	39	nm	<LOD	0.81	1.9	8	-
FU3-PL-11-TiD3	Fatu Kapa	Idef^X	Translucent smoker	1573	259	258	4.9	1.025	41	3.7	637	1.4	8.3	1142	509	49.8	15.5	35.0	541	612	78	<LOD	38	26	nm	<LOD	0.80	1.8	10	-
FU3-PL-11-TiG3	Fatu Kapa	Idef^X	Translucent smoker	1573	259	258	4.43	1.025	43	3.9	664	4.1	1.9	1268	518	63.5	2.0	44.7	733	802	110	160	nm	46	nm	2.5	0.78	1.9	8	1.848

Table 3: Continued.

Sample name	Zone	Site	Description	Depth	Tmax (sample) °C	Tmax (chimney) °C	pH	d^{20} Kg m^{-3}	S ‰	NaCl (wt%)	Cl mM	Si mM	SO_4 mM	Br μM	Na mM	K mM	Mg mM	Ca mM	Li μM	Li μM	Rb μM	Sr μM	Fe μM	Mn μM	Cu μM	Zn μM	Na/Cl	Br/Cl $\times 10^3$	Na/K	CH_4/Mn
FU3-PL-14-TiD1	Fatu Kapa	Idef[X]	Translucent smoker	1572	271	271	3.73	1.025	43	3.9	665	4.2	1.1	1282	519	66.2	0.8	43.4	764	823	120	144	28	64	nm	3.4	0.78	1.9	8	1.078
FU3-PL-14-TiG1	Fatu Kapa	Idef[X]	Translucent smoker	1572	271	271	3.97	1.025	42	3.9	661	4.1	0.8	1279	515	65.7	0.8	42.9	757	825	119	<LOD	nm	62	nm	<LOD	0.78	1.9	8	-
FU3-PL-14-TiD2	Fatu Kapa	Obel[X]	Translucent smoker	1669	272	-	4.59	1.03	49	4.5	769	4.5	0.7	1506	577	69.4	1.3	65.5	757	nm	nm	nm	nm	nm	nm	nm	0.75	2.0	8	-
FU3-PL-14-TiD3	Fatu Kapa	Obel[X]	Translucent smoker	1636	287	-	4.28	1.03	47	4.3	729	3.7	15.0	1283	557	58.8	11.1	65.0	621	nm	nm	nm	nm	nm	nm	nm	0.76	1.8	9	-
FU3-PL-14-TiG3	Fatu Kapa	Obel[X]	Translucent smoker	1636	287	-	5.37	1.028	43	3.9	672	2.5	27.0	1103	528	42.5	25.3	54.6	415	nm	nm	nm	nm	nm	nm	nm	0.79	1.6	12	-
FU3-PL-18-TiD1	Fatu Kapa	Aster[X]	Translucent smoker	1540	265	260	4.35	1.027	44	4.1	693	3.7	1.0	1344	533	64.9	1.2	51.1	755	nm	nm	nm	nm	nm	nm	nm	0.77	1.9	8	-
FU3-PL-17-TiD2	Fatu Kapa	Fati Ufu	Grey smoker	1522	299	303	4.26	1.031	47	4.3	739	3.3	9.3	1378	555	38.4	17.6	66.6	543	nm	nm	nm	nm	nm	nm	nm	0.75	1.9	14	-
FU3-PL-17-TiG2	Fatu Kapa	Fati Ufu	Grey smoker	1522	299	303	4.22	1.031	48	4.4	748	3.5	8.7	1402	562	39.8	15.9	69.7	569	nm	nm	nm	nm	nm	nm	nm	0.75	1.9	14	-
FU3-PL-21-TiD1	Fatu Kapa	Fati Ufu	Grey smoker	1523	302	301	3.81	1.032	50	4.6	784	4.7	1.4	1554	577	47.3	1.4	86.2	717	nm	nm	nm	nm	nm	nm	nm	0.74	2.0	12	-
FU3-PL-21-TiG1	Fatu Kapa	Fati Ufu	Grey smoker	1523	302	301	4.69	1.03	45	4.1	708	2.7	10.5	1292	544	34.7	19.3	60.3	474	nm	nm	nm	nm	nm	nm	nm	0.77	1.8	16	-
FU3-PL-21-TiD2	Fatu Kapa	Fati Ufu	White smoker	1503	-	284	3.27	1.028	44	4.1	694	4.9	0.4	1359	534	39.3	1.0	63.3	573	nm	nm	nm	nm	nm	nm	nm	0.77	2.0	14	-
FU3-PL-21-TiG2	Fatu Kapa	Fati Ufu	White smoker	1503	-	284	4.22	1.026	42	3.9	661	3.9	7.0	1217	520	32.0	13.3	50.6	435	nm	nm	nm	nm	nm	nm	nm	0.79	1.8	16	-
FU3-PL-20-TiD1	Fatu Kapa	Tutafi	Grey smoker	1580	316	317	4.1	1.029	46	4.2	720	2.6	0.6	1409	543	54.6	0.9	65.4	628	nm	nm	nm	nm	nm	nm	nm	0.75	2.0	10	-
FU3-PL-20-TiG1	Fatu Kapa	Tutafi	Grey smoker	1580	316	317	4.14	1.029	46	4.2	723	2.3	1.0	1409	543	54.7	0.7	66.4	630	nm	nm	nm	nm	nm	nm	nm	0.75	1.9	10	-
FU3-PL-21-TiD3	Fatu Kapa	Tutafi	White smoker	1626	293	294	2.92	1.028	45	4.1	701	5.1	0.9	1367	528	51.3	0.3	63.9	640	nm	nm	nm	nm	nm	nm	nm	0.75	1.9	10	-
FU3-PL-21-TiG3	Fatu Kapa	Tutafi	White smoker	1626	293	294	3.65	1.027	45	4.1	700	5.0	0.8	1371	528	51.0	0.8	63.3	633	nm	nm	nm	nm	nm	nm	nm	0.75	2.0	10	-

Table 4: Measured gas concentration and associated stable isotopic ratios hydrothermal fluids from the Kulo Lasi and Fatu Kapa vent fields. Values of log fH_2 were calculated using SUPCRT92 with the slop98 data base.

Sample name	Site	H_2S mM	N_2 mM	^3He mM	R/Ra	H_2 mM	log fH_2	CH_4 mM	CO_2 mM	C_2H_6 μM	C_2H_4 μM	C_3H_8 μM	C_3H_6 μM	n-C_4H_{10} μM	n-C_5H_{12} μM	δD (H_2) ‰	δD (CH_4) ‰	δ^{13}C (CO_2) ‰	δ^{13}C (CH_4) ‰	δ^{13}C (C_2H_6) ‰	δ^{13}C (C_3H_8) ‰	δ^{13}C (C_4H_{10}) ‰
Seawater			0.59	nm	nm	<LOD	-	<LOD	2.3	nm	nm	nm	nm	nm	nm	nm	nm	nm	nm	nm	nm	nm
FU-PL-05-TiG1	Kulo Lasi		0.12	nm	nm	<LOQ	-	0.001	2.6	<LOD	nm	<LOD	nm	<LOD	<LOD	nm	nm	nm	nm	nm	nm	nm
FU-PL-06-TiD4	Kulo Lasi	1.66	0.10	nm	nm	1.14	-	0.001	1.3	0.02	0.005	0.006	0.004	0.005	0.005	−323	n.m.	−3.2	−29	−27	−26	nm
FU-PL-06-TiG3	Kulo Lasi	5.05	1.43	nm	nm	19.8	−3.11	0.006	5.1	0.11	0.042	0.028	0.030	0.024	0.006	−306	n.m.	−4.1	−23	−26	−26	−24
FU-PL-06-TiD1	Kulo Lasi	0.39	2.48	nm	nm	6.18	−3.62	0.004	3.0	0.1	0.017	0.017	0.020	0.012	0.004	−300	n.m.	−1.9	−28	−24	−26	−24
FU-PL-06-TiG1	Kulo Lasi		0.79	nm	nm	1.04	−4.40	0.001	1.0	0.02	0.009	0.005	0.007	0.005	0.001	−316	n.m.	−0.2	−27.2	−22	−26	−24
FU3-PL-04-TiG3	Stéphanie	0.91	0.93	$1.1E-08$	8.6	0.03	−1.87	0.114	15.5	<LOD	<LOD	<LOD	<LOD	<LOD	1.7	nm	nm	nm	nm	nm	nm	nm
FU3-PL-08-TiD1	Stéphanie	1.23	1.98	nm		0.06	−1.57	0.235	29.0	<LOD	<LOD	<LOD	<LOD	<LOD	3.2	−676	−108	−5	−21.7	nm	nm	nm
FU3-PL-08-TiG1	Stéphanie	0.98	2.47	$4.4E-09$	7.6	0.05	−1.65	0.205	25.7	<LOD	<LOD	<LOD	<LOD	<LOD	2.9	nm	nm	nm	nm	nm	nm	nm
FU3-PL-09-TiD2	Stéphanie	0.23	0.48	$1.9E-09$	7.0	0.04	−1.75	0.059	6.0	<LOD	<LOD	<LOD	<LOD	<LOD	0.7	−436	−111	−5.3	−22.2	nm	nm	nm
FU3-PL-06-TiD1	Carla	1.34	0.50	$7.1E-09$	9.6	0.01	−2.35	0.021	4.5	<LOD	<LOD	<LOD	<LOD	<LOD	0.5	nm	nm	nm	nm	nm	nm	nm
FU3-PL-08-TiD3	Carla	0.19	3.33	$1.7E-08$	9.8	0.05	−1.65	0.066	11.9	<LOD	<LOD	<LOD	<LOD	<LOD	1.5	−410	−109	−4.7	−21.5	nm	nm	nm
FU3-PL-11-TiG3	Idef[X]	1.13	0.78	$1.8E-08$	9.8	0.03	−1.87	0.085	10.0	<LOD	<LOD	<LOD	<LOD	<LOD	1.1	nm	nm	nm	nm	nm	nm	nm
FU3-PL-14-TiD1	Idef[X]	1.00	1.20	$5.5E-09$	8.7	0.02	−2.05	0.069	10.1	<LOD	<LOD	<LOD	<LOD	<LOD	1.1	−417	−110	−4.9	−23.8	nm	nm	nm
FU3-PL-14-TiD2	Obel[X]	0.85	1.05	$3.8E-08$	9.8	0.03	−1.87	0.110	8.7	<LOD	<LOD	<LOD	<LOD	<LOD	1.0	−407	−113	−5	−24	nm	nm	nm
FU3-PL-14-TiD3	Obel[X]	0.54	0.93	$5.2E-09$	8.4	0.02	−2.05	0.165	9.2	<LOD	<LOD	<LOD	<LOD	<LOD	1.0	nm	nm	nm	nm	nm	nm	nm
FU3-PL-18-TiD1	Aster[X]	0.98	0.89	nm	nm	0.01	−2.35	0.067	9.2	<LOD	<LOD	<LOD	<LOD	<LOD	1.0	−412	−111	−4.9	−23.6	nm	nm	nm
FU3-PL-17-TiG2	Fati Ufu	1.76	0.84	$2.7E-08$	9.9	0.01	−2.59	0.070	21.5	<LOD	<LOD	<LOD	<LOD	<LOD	2.3	-	−93	−2.3	−6.1	nm	nm	nm
FU3-PL-21-TiD2	Fati Ufu	0.71	2.07	$3.1E-09$	9.9	0.03	−2.11	0.111	12.6	<LOD	<LOD	<LOD	<LOD	<LOD	1.5	−410	−109	−4.4	−23.3	nm	nm	nm
FU3-PL-20-TiD1	Tutafi	2.36	1.18	$1.4E-08$	9.2	0.05	−1.89	0.156	22.2	<LOD	<LOD	<LOD	<LOD	<LOD	2.4	−396	−111	−4.5	−23.6	nm	nm	nm
FU3-PL-21-TiD3	Tutafi	0.84	1.67	nm	nm	0.03	−2.11	0.053	11.7	<LOD	<LOD	<LOD	<LOD	<LOD	1.4	−415	−109	−4.7	−24.2	nm	nm	nm

Table 5: Endmember compositions in fluids from the Kulo Lasi and Fatu Kapa vent fields. Kulo Lasi endmembers cannot be extrapolated at Mg = 0. Values presented here for both brine and condensed vapour phases correspond to concentrations in the fluid with the lowest Mg. Elemental compositions in endmember fluids from the various sites of the Fatu Kapa vent field were calculated using the mixing lines (Figure S1) and assuming Mg = 0. Values of the purest fluid were used when linear regression was not possible (*). Note that only one sample was available for the Aster^{X} site (1).

Zone	Site	Depth	T °C	pH	NaCl (wt%)	Cl mM	Si mM	SO4 mM	Br μM	Na mM	K mM	Mg mM	Ca mM	Li μM	Rb μM	Sr μM	Fe μM	Mn μM	Cu μM	Zn μM	Na/Cl	Br/Cl $\times 10^3$	Na/K	CH4/Mn
Kulo Lasi	NaCl poor	1475	345	2.24	2.9	497	8.2	8.8	738	388	18.5	24.6	11.6	149	26	7.3	4796	862	14	45	0.78	1.48	21	0.007*
Kulo Lasi	NaCl rich	1475	345	2.36	4.3	735	14.6	6.2	1135	612	29.5	26.5	10.9	238	46	3.4	9884	1416	2.5	175	0.83	1.54	21	0.001*
Fatu Kapa	Stéphanie	1555	280	3.4	4.5	767	4.7*	0.0	1569	532	54.5	0.0	98.9	708	114	282*	655*	268	6.6*	<LOD	0.69	2.05	10	0.76*
Fatu Kapa	Carla	1664	280	2.8	3.5	594	4.3	0.0	1132	477	59.9	0.0	31.4	691	105	114*	287*	53	nm	4.4*	0.80	1.90	8	1.37*
Fatu Kapa	Idef^{X}	1572	270	3.7	3.9	665	4.2*	0.0	1282	518	66.4	0.0	44.3	751	113	160*	28*	60	nm	3.4*	0.78	1.93	8	1.08*
Fatu Kapa	Obel^{X}	1669	270	4.6	4.5	771	4.6	0.0	1458	580	71.0	0.0	85.9	777	nm	nm	nm	nm	nm	nm	0.75	1.89	8	-
Fatu Kapa	Aster^{X}(1)	1540	265	4.4	4.1	693	3.7	1.0	1344	533	64.9	1.2	51.1	755	nm	nm	nm	nm	nm	nm	0.77	1.94	8	-
Fatu Kapa	Fati Ufu	1523	300	3.8	4.6	790	4.9	0.0	1589	580	48.2	0.0	85.4	722	nm	nm	nm	nm	nm	nm	0.73	2.01	12	-
Fatu Kapa	Fati Ufu	1503	280	3.3	4.1	700	4.9	0.0	1380	538	40.0	0.0	65.0	583	nm	nm	nm	nm	nm	nm	0.77	1.97	13	-
Fatu Kapa	Tutafi	1580	315	4.1	4.2	713	5.1	0.0	1405	535	52.9	0.0	65.1	635	nm	nm	nm	nm	nm	nm	0.75	1.97	10	-
IAPSO	Standard sw	-	-	-	3.2	546	0.0	28.2	839	468	10.2	53.2	10.3	27	1.3	90	<LOD	<LOD	<LOD	<LOD	0.9	1.5	46	-
Kulo Lasi	Reference sw	1150	-	-	3.2	551	0.1	29.0	833	457	9.8	53.2	10.6	25	4.4	93	<LOD	<LOD	<LOD	<LOD	0.83	1.5	47	-
Fatu Kapa	Reference sw	1488	-	-	3.3	565	0.0	28.8	841	483	10.4	54.5	10.7	22	5.8	<LOD	<LOD	<LOD	<LOD	<LOD	0.85	1.5	46	-
Fatu Kapa	Reference sw	1572	2	-	3.3	557	0.0	28.7	841	477	10.4	54.2	10.8	23	nm	nm	nm	nm	nm	nm	0.86	1.5	46	-

*Maximum value when linear regression was not possible; (1) only one sample.

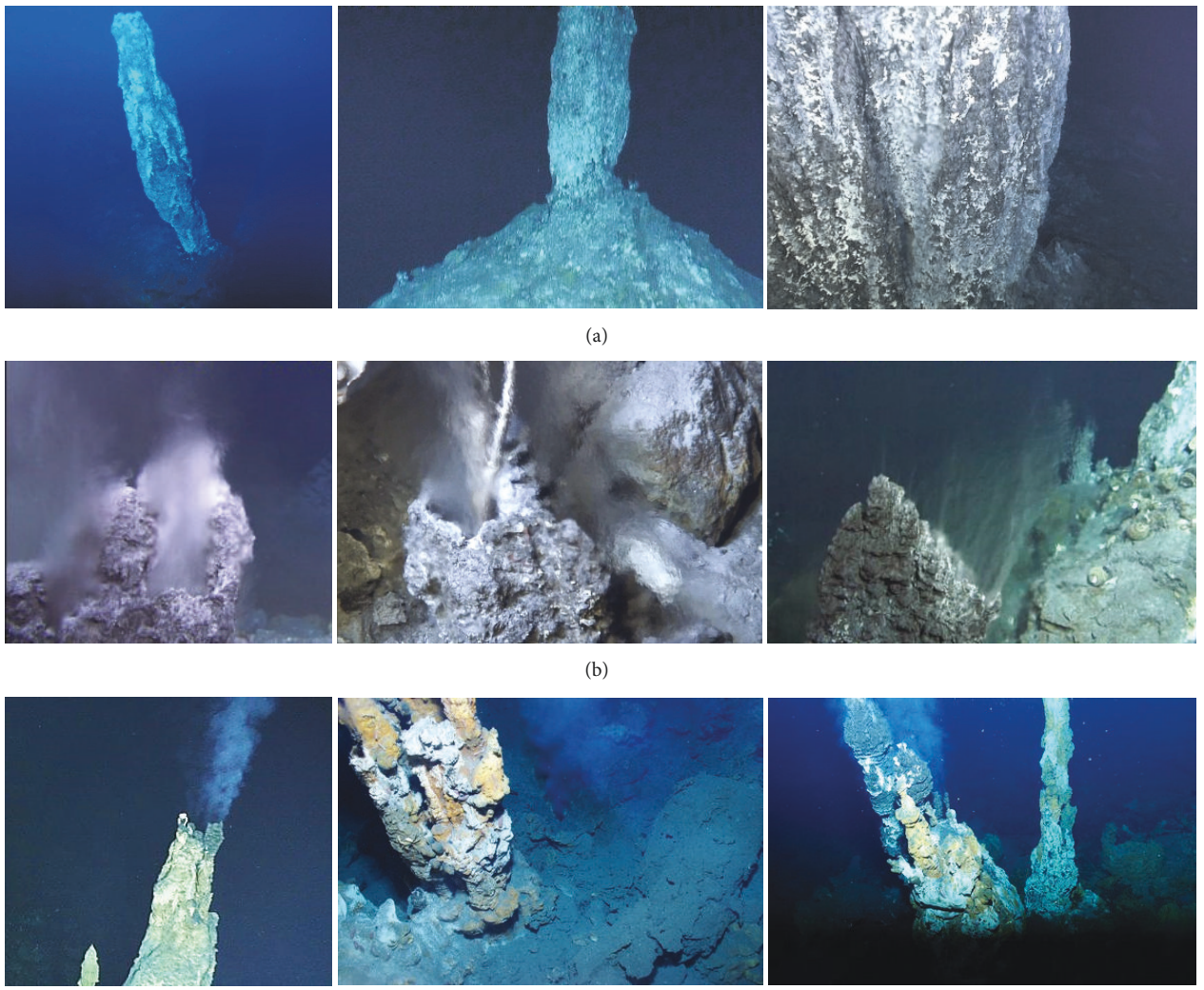

(a)

(b)

(c)

Figure 3: (a) and (b) Photographs of anhydrite structures observed at Stéphanie, Carla, Idef^X, Aster^X, and Obel^X site. (c) Photographs of grey smokers associated with sulphides structures observed at Fati Ufu and Tutafi. Copyrights from Ifremer, FUTUNA 3 cruise.

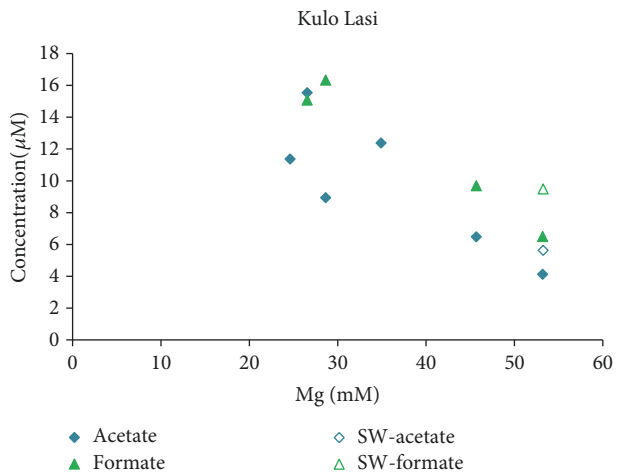

Figure 4: Mixing lines of formate and acetate versus Mg for the Kulo Lasi fluids. Note that the reference deep-sea water sample (FU-PL05-TiG2 noted as SW here) was taken at 1150 m depth above the southern wall of the caldera (see Figure 1 for location and Table 3) and thus very likely within the plume [7]. This would account for the unusual concentrations of formate and acetate detected.

Carla. Acetate was detected in all analysed samples and concentrations were an order of magnitude higher than the ones of formate (543–2309 ppb) (Table 6).

Heavier extractable organic compounds were not detected in the dry control experiment and only a few were detectable but below limit of quantification (LOQ) in the MQ water blank experiment (Table 6). This showed that sample preparation and storage could be considered as contamination-free steps. The levels of heavier extractable organic compounds appeared rather high in the reference water at Fatu Kapa certainly because of the overall spread hydrothermal discharges and diffuse venting in the region [7] (Table 6, Figure 5). This sample was indeed taken mid-way between Obel^X and Aster^X fields at about 20 m above the seafloor. As a consequence, it is difficult to assess possible contamination originating from sampling device or seawater contribution in the present case. However, earlier studies have shown that they generally did not represent major sources of contamination as for the studied compounds [27, 37]. Nevertheless, in comparison to deep-sea water both the qualitative (Kulo Lasi) and quantitative (Fatu Kapa) data obtained suggested enrichment of the fluids in hydrothermally derived compounds, namely, n-alkanes (C_9–C_{12}), n-FAs (C_9, C_{12}, C_{14}–C_{18}), and PAHs (fluorene, phenanthrene, pyrene) ([39]; Table 6, Figures 5 and 6). Such enrichment was unclear for >C_{12} n-alkanes; C_{10}, C_{11}, C_{13} n-FAs; BTEXs; naphthalene, acenaphthene, and fluoranthene because of their very low concentration and/or the measurement uncertainty.

Differences in concentrations seemed to exist among the vents over the Fatu Kapa area. Fluids from the Stéphanie vent field had concentrations in hydrocarbons equal or below the reference water sample whereas they were clearly enriched in C_9, C_{12}, C_{14}–C_{18} n-FAs. The Carla fluids were slightly enriched in C_9–C_{12} n-alkanes and showed the highest concentrations in PAHs. Fluids from Idef^X, Fati Ufu, and Tutafi shared some similarities: a strong enrichment in decane and undecane, alike concentrations in PAHs, and the presence of significant amounts of xylene. However, fluids expelled at the Tutafi vent appeared the most enriched in C_9–C_{11} n-alkanes and xylenes. In terms of fatty acids and considering the analytical error, the 5 vents showed consistent concentrations with C_9, C_{16}, and C_{18} being major. Note that fluids from Fati Ufu seemed depleted in C_{17} and C_{18}.

Generally we did not observe strong linear correlation between the concentration of individual compounds and Mg. Nonetheless, these relations showed that both enrichment and depletion of organic compounds seemed to occur in hydrothermal fluids versus deep-sea water.

5. Discussion

The elemental and gas composition of hydrothermal fluids is mainly affected by water/rock interactions and thus the nature of the host rocks, phase separation, magmatic fluid contribution, conductive cooling, and seawater mixing in local recharge zones [45]. In the following discussion we attempt to unravel the occurrence of these various processes both at Kulo Lasi and at Fatu Kapa. Much less is known on processes that control organic geochemistry and are therefore discussed here as well as some implications of the presence of organic compounds in hydrothermal fluids. Implications related to the composition of the fluids are dependent on fluxes; therefore, we give here an attempt to provide order of magnitude estimates of heat and mass fluxes.

5.1. Plume-Fluids Relations. The geochemistry and dynamics of the plumes over the Wallis and Futuna region have been studied elsewhere [7]. The Kulo Lasi plume has been proposed to be the result of both high-T and diffuse venting from multiple vents located both on the floor and on the wall of the caldera. Consistently, both types of venting have been observed [6]. Helium, nephelometry, and Mn profiles recorded above the northern sampling area showed constant elevated concentrations in the 300 masf and were assumed to be the results of diffuse venting. Our results show that they are obviously the result of the numerous small black smokers observed on the seafloor (Figure 2). The methane concentration in the sampled fluids was extremely low which cannot account for the elevated concentration of CH_4 in the water column reported by Konn et al. [7]. The strong difference in the CH_4/Mn ratios between the plume (0.7–4.5) and the sampled fluids (0.001–0.01) is another line of evidence that the methane plume has another origin compared to hydrothermal fluids and likely come from degassing of the lava flows as suggested by the authors. Although other fluid discharges likely remain undiscovered, this is consistent with a past eruption and accumulation of the water mass in the caldera [39].

A great diversity of the fluid compositions was expected from the geological settings and the water column survey and was indeed confirmed by the mixing lines that point to as many endmembers as sampled areas (Figure S1). CH_4/TDM ratios also differed among the vents but it was not due to sole CH_4 concentration variations as suggested earlier (Table 5) [7]. Finally, the very weak nephelometry of the Fatu Kapa plume is likely best explained by the low metal contents of the fluids.

5.2. Reaction Zone Depth. The solubility of Quartz in hydrothermal fluids has been studied by different authors (e.g., [46]). According to these works silica concentration in the fluid may be used to estimate the depth of the reaction zone. The silica concentration measured in the Kulo Lasi and Fatu Kapa fluids indicates a hydrothermal reaction zone at seafloor or in the water column (Figure S2). Both observations suggest that, in this area, fluids are not in equilibria with Quartz at the pressure and temperature of the fluid emission. And this prevents using Si as a geothermometer to determine the depth of the reaction zone.

All fluids at Fatu Kapa were indeed highly depleted in Si with respect to the Quartz saturation curve at 170 bar, 300°C (Si ~12 mM in Figure S2). A higher temperature in the reaction zone (>350°C at 200 bar) may explain a lower Si concentration in the fluid at equilibrium as Quartz solubility decreases (Figure S2). The dispersion of a great number of

Table 6: Measured concentration of Total Organic Carbon (TOC), formate, acetate, and a selection of individual semi-volatile organic compounds extracted from hydrothermal fluids of the Kulo Lasi and Fatu Kapa vent fields.

Compound	Rt min	Units	Blank Dry	Blank MQ	FU3-PL-14-TiG2 deepsea water	FU3-PL-08-TiD2 Stéphanie	FU3-PL-04-TiD3 Stéphanie	FU3-PL-09-TiG2 Stéphanie	FU3-PL-08-TiG3 Carla	FU3-PL-06-TiG1 Carla	FU3-PL-14-TiG1 Idefix	FU3-PL-11-TiD3 Idefix	FU3-PL-21-TiG2 Fati Ufu	FU3-PL-17-TiD2 Fati Ufu	FU3-PL-21-TiG1 Fati Ufu	FU3-PL-21-TiG3 Tutafi	FU3-PL-20-TiG1 Tutafi
pH	-		-	-	-	3.83	4.65	5.42	4.17	4.91	3.97	4.9	4.22	4.26	4.69	3.65	4.14
Mg	-	mM	-	-	54.2	0.6	18.7	44.3	2.7	23.6	0.8	15.5	13.3	17.6	19.3	0.8	0.7
TOC	-	ppm	na	<0.005	na	0.165	na	na	na	na	0.498	na	na	6.514	na	0.304	na
Formate	-	ppb	na	nd	na	65.8	<LOQ	na	na	na	<LOQ	<LOQ	111.7	721.6	na	<LOQ	na
Acetate	-	ppb	na	nd	na	1155.1	543.2	na	na	na	1033.6	995.1	1740.9	2308.8	na	1067.3	na
Nonane	4.68	ppb	nd	nd	0.85 ± 0.51	1.59 ± 0.52	1.17 ± 0.51	1.08 ± 0.51	0.72 ± 0.51	0.58 ± 0.51	0.84 ± 0.51	0.52 ± 0.50	0.64 ± 0.50	0.50 ± 0.51	0.28 ± 0.51	1.52 ± 0.52	2.29 ± 0.54
Decane	5.911	ppb	nd	<0.03	2.21 ± 0.44	2.03 ± 0.44	2.02 ± 0.44	2.10 ± 0.44	3.05 ± 0.45	1.63 ± 0.44	6.92 ± 0.51	2.20 ± 0.44	6.47 ± 0.50	5.58 ± 0.48	2.88 ± 0.45	9.18 ± 0.56	22.16 ± 0.95
Undecane	7.183	ppb	nd	<0.2	11.35 ± 0.97	6.79 ± 0.76	9.52 ± 0.87	11.48 ± 0.98	13.81 ± 1.14	9.61 ± 0.87	23.13 ± 1.88	10.89 ± 0.94	19.13 ± 1.55	26.06 ± 2.14	12.26 ± 1.03	20.48 ± 1.66	26.93 ± 2.21
Dodecane	8.394	ppb	nd	nd	3.36 ± 0.65	1.33 ± 0.57	2.30 ± 0.60	2.98 ± 0.63	3.35 ± 0.65	2.64 ± 0.61	5.12 ± 0.76	3.35 ± 0.65	4.76 ± 0.73	6.52 ± 0.86	3.30 ± 0.65	4.00 ± 0.69	5.14 ± 0.76
Tridecane	9.549	ppb	nd	nd	1.39 ± 0.54	0.35 ± 0.53	0.73 ± 0.53	0.86 ± 0.53	1.37 ± 0.54	1.39 ± 0.54	1.63 ± 0.55	2.21 ± 0.57	1.75 ± 0.55	3.89 ± 0.65	2.27 ± 0.57	1.06 ± 0.54	1.42 ± 0.54
Tetradecane	10.641	ppb	nd	nd	0.53 ± 0.47	0.56 ± 0.47	0.57 ± 0.47	0.59 ± 0.47	0.67 ± 0.46	0.66 ± 0.46	0.59 ± 0.47	0.72 ± 0.46	0.69 ± 0.46	0.64 ± 0.46	0.72 ± 0.46	0.72 ± 0.46	0.70 ± 0.46
Pentadecane	11.675	ppb	nd	nd	0.44 ± 0.28	0.40 ± 0.28	0.48 ± 0.27	0.44 ± 0.28	0.52 ± 0.27	0.59 ± 0.27	0.43 ± 0.28	0.60 ± 0.27	0.57 ± 0.27	0.47 ± 0.28	0.49 ± 0.27	0.62 ± 0.27	0.58 ± 0.27
Hexadecane	12.65	ppb	nd	nd	0.25 ± 0.73	0.40 ± 0.74	0.42 ± 0.73	0.49 ± 0.73	0.64 ± 0.73	0.59 ± 0.74	0.26 ± 0.73	0.84 ± 0.74	0.53 ± 0.73	0.39 ± 0.73	0.37 ± 0.73	0.65 ± 0.74	0.48 ± 0.73
Heptadecane	13.576	ppb	nd	nd	0.57 ± 0.32	1.08 ± 0.32	0.61 ± 0.32	0.87 ± 0.32	1.13 ± 0.33	0.85 ± 0.32	1.20 ± 0.33	1.48 ± 0.33	0.85 ± 0.32	0.67 ± 0.32	0.78 ± 0.32	1.10 ± 0.33	0.98 ± 0.32
Octadecane	14.452	ppb	nd	nd	0.17 ± 0.17	0.30 ± 0.18	0.28 ± 0.18	0.30 ± 0.18	0.35 ± 0.18	0.33 ± 0.18	0.39 ± 0.18	0.42 ± 0.18	0.49 ± 0.19	0.29 ± 0.18	0.25 ± 0.18	0.47 ± 0.18	0.50 ± 0.19
Nonadecane	15.295	ppb	nd	nd	1.08 ± 1.34	1.36 ± 1.35	1.24 ± 1.35	1.38 ± 1.34	1.64 ± 1.36	1.40 ± 1.36	1.33 ± 1.35	1.83 ± 1.38	1.26 ± 1.33	0.86 ± 1.33	1.02 ± 1.34	1.10 ± 1.33	1.36 ± 1.35
Eicosane	16.104	ppb	nd	nd	1.09 ± 1.23	1.75 ± 1.27	1.05 ± 1.25	0.94 ± 1.23	1.13 ± 1.24	1.69 ± 1.27	1.03 ± 1.24	1.46 ± 1.26	1.00 ± 1.23	0.71 ± 1.24	1.19 ± 1.24	1.25 ± 1.24	1.50 ± 1.26
Nonanoic acid	6.914	ppb	nd	nd	3.72 ± 2.53	8.07 ± 2.96	<0.37	5.71 ± 2.67	4.49 ± 2.56	3.49 ± 2.50	4.91 ± 2.60	7.12 ± 2.87	8.94 ± 3.09	9.23 ± 3.10	na	2.86 ± 2.45	9.90 ± 3.21
Decanoic acid	7.542	ppb	nd	nd	1.17 ± 1.65	0.86 ± 1.59	nd	0.53 ± 1.60	0.41 ± 1.65	nd	0.61 ± 1.62	nd	0.84 ± 1.67	0.56 ± 1.68	na	1.09 ± 1.64	0.83 ± 1.66
Undecanoic acid	8.178	ppb	nd	nd	0.18 ± 0.19	0.29 ± 0.20	nd	0.23 ± 0.19	0.25 ± 0.20	0.28 ± 0.19	0.22 ± 0.20	nd	0.26 ± 0.19	0.34 ± 0.19	na	0.35 ± 0.20	0.33 ± 0.19
Dodecanoic acid	8.773	ppb	nd	nd	0.42 ± 0.48	2.10 ± 0.51	0.55 ± 0.48	0.55 ± 0.48	0.78 ± 0.48	0.49 ± 0.47	2.01 ± 0.51	0.69 ± 0.48	1.29 ± 0.49	1.08 ± 0.49	na	1.45 ± 0.49	0.61 ± 0.48
Tridecanoic acid	9.31	ppb	nd	nd	0.28 ± 0.20	0.35 ± 0.19	0.23 ± 0.21	0.24 ± 0.21	0.24 ± 0.20	0.33 ± 0.20	0.27 ± 0.20	0.25 ± 0.21	0.26 ± 0.21	0.32 ± 0.20	na	0.31 ± 0.19	0.27 ± 0.20
Tetradecanoic acid	9.859	ppb	nd	<0.06	0.94 ± 0.32	1.86 ± 0.31	1.44 ± 0.31	0.87 ± 0.33	0.92 ± 0.32	4.28 ± 0.35	1.41 ± 0.31	2.74 ± 0.31	0.90 ± 0.32	1.15 ± 0.32	na	1.42 ± 0.31	1.07 ± 0.32
Pentadecanoic acid	10.355	ppb	nd	nd	0.54 ± 0.30	1.44 ± 0.30	0.82 ± 0.28	0.46 ± 0.30	0.76 ± 0.29	0.57 ± 0.29	1.06 ± 0.29	0.58 ± 0.30	0.52 ± 0.30	0.78 ± 0.29	na	1.02 ± 0.29	0.77 ± 0.29
Hexadecanoic acid	10.902	ppb	nd	nd	1.46 ± 1.20	6.66 ± 1.37	4.47 ± 1.27	1.78 ± 1.20	3.90 ± 1.25	2.91 ± 1.23	7.30 ± 1.41	3.61 ± 1.24	3.24 ± 1.23	4.92 ± 1.29	na	6.09 ± 1.34	5.59 ± 1.32
Heptadecanoic acid	11.317	ppb	nd	nd	0.54 ± 0.61	3.23 ± 0.58	nd	0.89 ± 0.53	2.04 ± 0.54	1.82 ± 0.54	1.04 ± 0.62	1.62 ± 0.55	<0.03	2.89 ± 0.59	na	2.87 ± 0.59	2.79 ± 0.57
Octadecanoic acid	11.78	ppb	nd	nd	0.94 ± 2.16	8.70 ± 2.82	6.32 ± 2.55	1.67 ± 2.32	6.36 ± 2.48	3.49 ± 2.30	11.83 ± 3.29	5.15 ± 2.35	2.64 ± 2.09	5.26 ± 2.40	na	9.19 ± 2.86	9.66 ± 2.96
Ethyl, Benzene	4.344	ppb	nd	<0.1	nd	<0.1	<0.1	nd	nd	<0.1	<0.1	na	0.10 ± 0.35	<0.1	<0.1	nd	0.44 ± 0.23
p-,m-Xylene	4.443	ppb	nd	nd	0.03 ± 0.05	0.10 ± 0.05	0.11 ± 0.05	0.08 ± 0.05	0.10 ± 0.05	0.11 ± 0.05	0.18 ± 0.05	na	0.33 ± 0.05	0.21 ± 0.05	0.15 ± 0.05	0.11 ± 0.05	0.71 ± 0.08
o-Xylene	4.708	ppb	nd	<0.02	0.02 ± 0.05	0.07 ± 0.06	0.06 ± 0.05	0.02 ± 0.06	0.03 ± 0.08	0.06 ± 0.05	0.14 ± 0.06	na	0.33 ± 0.07	0.19 ± 0.06	0.13 ± 0.06	0.06 ± 0.05	0.68 ± 0.09

Table 6: Continued.

Compound	Rt min	Units	Blank Dry	Blank MQ	FU3-PL-14-TiG2 deepsea water	FU3-PL-08-TiD2 Stéphanie	FU3-PL-04-TiD3 Stéphanie	FU3-PL-09-TiG2 Stéphanie	FU3-PL-08-TiG3 Carla	FU3-PL-06-TiG1 Carla	FU3-PL-14-TiG1 Idefix	FU3-PL-11-TiD3 Idefix	FU3-PL-21-TiG2 Fati Ufu	FU3-PL-17-TiD2 Fati Ufu	FU3-PL-21-TiG1 Fati Ufu	FU3-PL-21-TiG3 Tutafi	FU3-PL-20-TiG1 Tutafi
Styrene	4.831	ppb	nd	nd	0.59 ± 0.14	0.22 ± 0.16	nd	nd	0.46 ± 0.14	nd	0.29 ± 0.15	na	0.21 ± 0.15	0.20 ± 0.15	0.24 ± 0.14	0.37 ± 0.14	0.20 ± 0.14
isopropyl, Benzene	5.006	ppb	nd	nd	0.04 ± 0.05	0.06 ± 0.05	0.07 ± 0.05	0.07 ± 0.05	0.06 ± 0.05	0.08 ± 0.05	0.09 ± 0.05	na	0.09 ± 0.05	0.04 ± 0.06	0.05 ± 0.05	0.09 ± 0.05	0.09 ± 0.05
n-Propyl, Benzene	5.468	ppb	nd	nd	0.03 ± 0.04	0.02 ± 0.04	0.03 ± 0.04	0.02 ± 0.04	0.03 ± 0.04	0.03 ± 0.04	0.03 ± 0.04	na	0.04 ± 0.04	0.03 ± 0.04	0.03 ± 0.05	0.03 ± 0.04	0.04 ± 0.04
1,2,4-triMethyl-Benzene	5.572	ppb	nd	nd	0.03 ± 0.04	0.05 ± 0.04	0.06 ± 0.04	0.04 ± 0.04	0.06 ± 0.05	0.06 ± 0.04	0.04 ± 0.05	na	0.08 ± 0.04	0.07 ± 0.05	0.07 ± 0.04	0.08 ± 0.04	0.07 ± 0.04
1,3,5-triMethyl-Benzene	5.95	ppb	nd	nd	0.02 ± 0.06	0.11 ± 0.07	0.08 ± 0.07	0.06 ± 0.06	0.09 ± 0.06	0.09 ± 0.06	0.11 ± 0.06	na	0.30 ± 0.07	0.25 ± 0.06	0.20 ± 0.07	0.13 ± 0.06	0.19 ± 0.06
sec-Butyl-Benzene	6.106	ppb	nd	nd	0.27 ± 0.05	0.04 ± 0.04	nd	0.04 ± 0.05	0.05 ± 0.06	0.05 ± 0.05	0.06 ± 0.05	na	nd	0.05 ± 0.05	nd	nd	0.07 ± 0.05
2,isopropyl, Toluene	6.305	ppb	nd	nd	0.07 ± 0.03	0.03 ± 0.03	0.03 ± 0.03	0.03 ± 0.03	0.05 ± 0.03	0.03 ± 0.03	0.04 ± 0.03	na	0.04 ± 0.03	0.04 ± 0.03	0.03 ± 0.03	0.05 ± 0.03	0.07 ± 0.03
n-Butyl, Benzene	6.66	ppb	nd	<0.08	0.06 ± 0.03	0.01 ± 0.03	0.01 ± 0.02	0.01 ± 0.03	0.02 ± 0.03	0.01 ± 0.02	0.02 ± 0.02	na	0.02 ± 0.03	0.02 ± 0.02	nd	0.03 ± 0.03	0.03 ± 0.03
Naphthalene	8.351	ppb	nd	<0.01	1.39 ± 0.07	0.49 ± 0.05	0.32 ± 0.05	0.13 ± 0.04	1.24 ± 0.07	0.69 ± 0.05	1.08 ± 0.06	na	0.90 ± 0.06	0.64 ± 0.05	1.99 ± 0.09	1.19 ± 0.06	1.19 ± 0.06
Acenaphthene	11.796	ppb	nd	nd	<0.009	<0.009	<0.009	<0.009	<0.009	<0.009	<0.009	na	<0.009	<0.009	<0.009	<0.009	<0.009
Fluorene	12.778	ppb	nd	nd	nd	0.05 ± 0.03	<0.01	<0.01	0.14 ± 0.03	0.10 ± 0.03	0.16 ± 0.03	na	0.14 ± 0.03	0.09 ± 0.03	0.06 ± 0.03	0.09 ± 0.03	0.07 ± 0.03
Phenanthrene	14.582	ppb	nd	nd	0.02 ± 0.04	0.10 ± 0.04	0.06 ± 0.04	0.06 ± 0.04	0.29 ± 0.05	0.13 ± 0.04	0.20 ± 0.05	na	0.16 ± 0.05	0.10 ± 0.04	0.06 ± 0.04	0.23 ± 0.05	0.17 ± 0.05
Anthracene	14.788	ppb	nd	nd	nd	nd	nd	nd	nd	nd	nd	na	nd	nd	nd	nd	nd
Fluoranthene	17.117	ppb	nd	nd	<0.04	<0.04	<0.04	<0.04	0.06 ± 0.16	<0.04	<0.04	na	0.04 ± 0.16	<0.04	<0.04	0.05 ± 0.16	<0.04
Pyrene	17.52	ppb	nd	nd	<0.03	0.03 ± 0.11	0.03 ± 0.10	<0.03	0.14 ± 0.11	0.07 ± 0.10	0.10 ± 0.11	na	0.06 ± 0.10	0.05 ± 0.11	0.03 ± 0.10	0.09 ± 0.10	0.06 ± 0.10

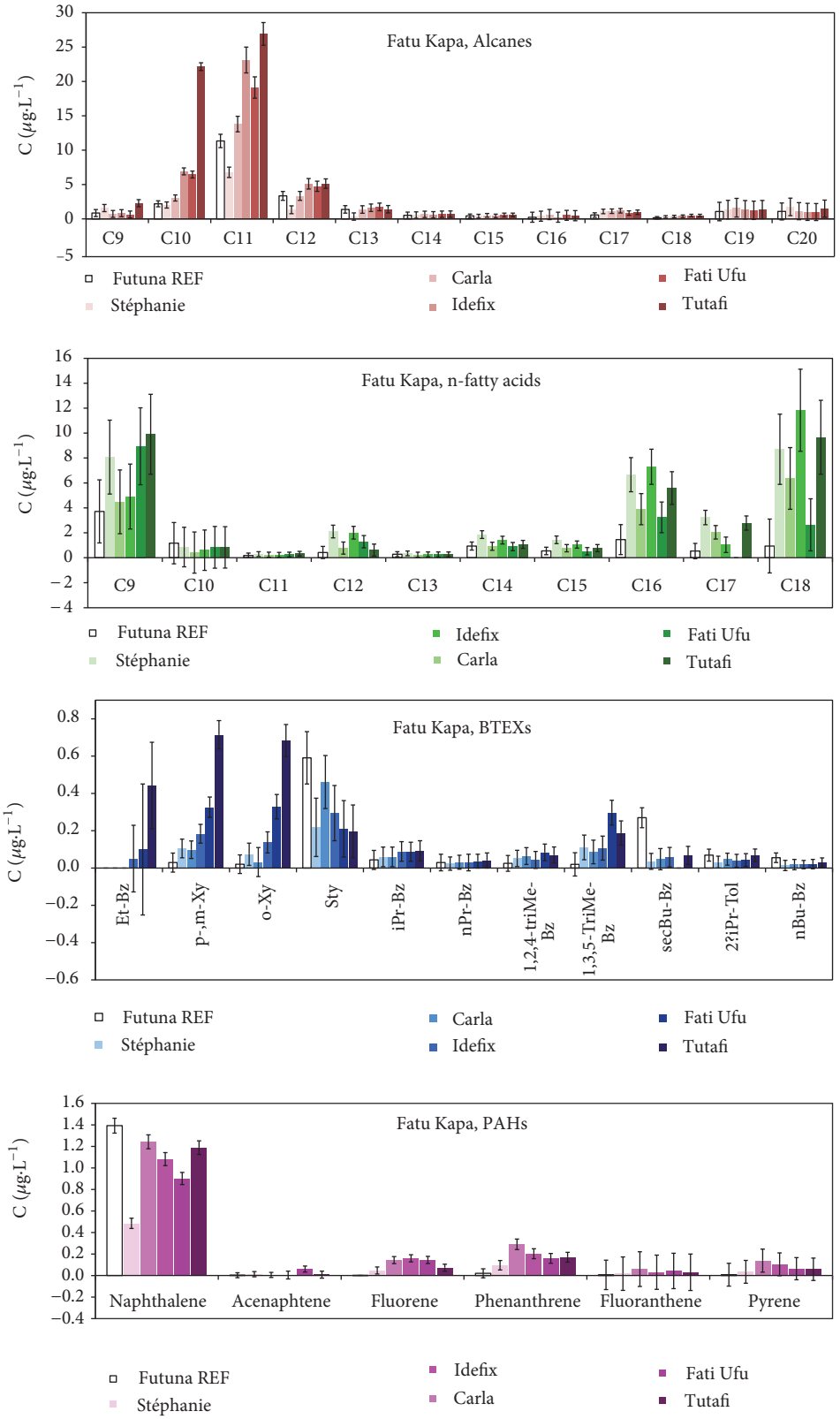

Figure 5: Distribution of n-alkanes, n-fatty acids, mono-, and polyaromatic hydrocarbons (BTEX and PAH) in the purest fluids of the Stéphanie, Carla, Idef^{X}, Fati Ufu, and Tutafi sites collected within the Fatu Kapa vent field. Because organic geochemistry does not seem to follow a simple mixing model, endmember concentrations cannot be calculated. To that respect composition of the purest fluids is presented and assumed to be close to endmembers composition. Note that quantitative results are not available for the Kulo Lasi fluids (see Figure 6 for chromatograms).

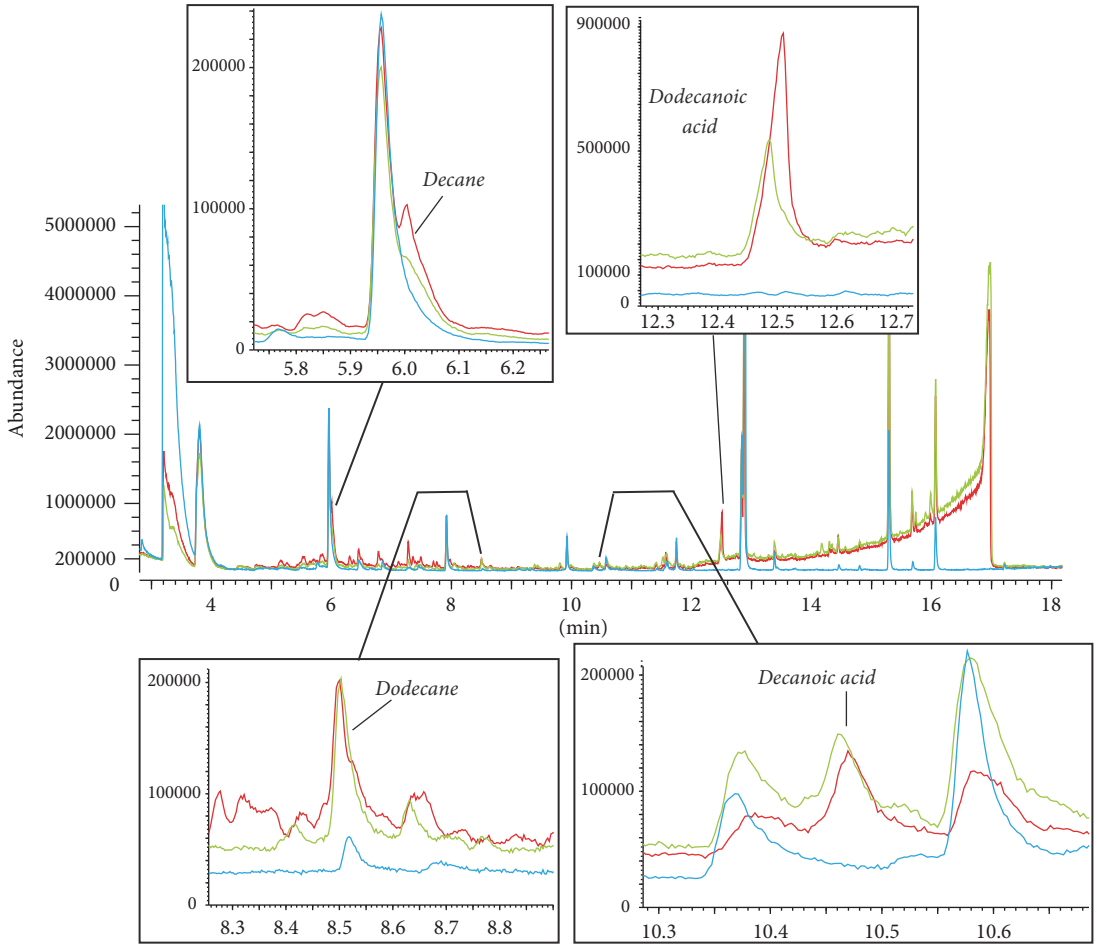

FIGURE 6: Only qualitative results could be obtained at Kulo Lasi. This figure presents a selection of representative chromatograms obtained for the Kulo Lasi fluid samples. For the sake of clarity, close-ups of a few peaks are shown to illustrate the enrichment of fluids (FU-PL06-TiG1 in red and FU-PL06-TiD3 in green) versus the reference deep-sea water (FU-PL05-TiG2 in blue).

vent fields over a large area of recent lava flows may be due to complex fluid pathways that favour conductive cooling of the fluid and subsurface loss of silica before venting on the seafloor. Consistently, amorphous silica was common in the seafloor deposits at Fatu Kapa where opal was abundant as a late mineral in sulphides and as silica crusts (slabs) at the surface of the deposits [6]. In conclusion, this would indicate a fairly shallow reaction zone at Fatu Kapa (a few 100 mbsf) in agreement with the geological settings and the possible occurrence of dikes.

5.3. Chlorinity. Phase separation is often accounted for salinity deviation in hydrothermal fluids versus seawater [47, 48]. Phase separation is of great importance in metal transportation and ore-forming processes, for example, [24, 49–51]. It also implies that seawater experiences dramatic changes in its physical and chemical properties as it reaches the super- or subcritical state. In particular, strong modification of the density and ionic strength of seawater enables unconventional chemical reactions, hence a likely importance in hydrothermal organic geochemistry, for example, [52]. The measured P and T of the Kulo Lasi fluids are almost on the critical curve of seawater meaning that liquid and vapor phase may coexist at Kulo Lasi. An adiabatic decompression of supercritical seawater (initial fluid and equivalent to 3.2 wt% NaCl) as it rises towards the seafloor would cause it to separate, at about 320–350 bar and 415–420°C, into two phases having the NaCl percentages observed at Kulo Lasi (Figure S3) [53, 54].

Similarly, the excess salinity of the Fatu Kapa fluids (9 to 41%) could be explained by phase separation and is supported by the Br/Cl ratios which significantly differed from seawater [45, 55]. Since we have not sampled any Cl-depleted fluids we may infer that phase separation may have occurred in the past and that only the brine phase was venting at the time of the cruise. Alternatively water-rock reactions could represent a significant Cl source to the fluids [56]. Indeed, the felsic lavas collected in the Fatu Kapa area contained up to 10 times more Cl than MORB *(Aurélien Jeanvoine, personal communication)*.

5.4. Water-Rock Reactions. Generally, fluids from Kulo Lasi and Fatu Kapa were not typical of back-arc settings but shared similarities with ridge, arc, and back-arc settings fluid

signatures [3]. The Kulo Lasi fluids have unusually high concentrations of Mg (24.6 to 34.9 mM) and SO_4 (6.2 to 12.0 mM) at low pH (2.24 to 3.32) and high T (338–343°C) which indicate that significant seawater mixing at subsurface or during sampling is rather unlikely. In back-arc context, the occurrence of Mg and SO_4 in endmember fluids can be explained by a magmatic fluid input as observed at the Desmos [5, 57], Rota 1 and Brother sites [58, 59]. Magmatic-derived SO_2 would disproportionate according to reaction (1) at temperatures measured at Kulo Lasi (e.g., [5, 60]). This is consistent with widespread occurrences of native sulfur on fresh lava near the active vents [39] as well as the low pH of the fluids.

$$3SO_2\,(aq) + 2H_2O = S^0\,(s) + 4H^+ + 2SO_4 \quad (1)$$

Yet CO_2 concentrations are low and the Na : K : Mg ratios are strongly different to seawater. The latter suggests a contribution of Mg by dissolution of magnesium silicates [39]. Besides, the high Li and Rb concentrations and the presence of recent lava injected in the caldera point to water/fresh hot volcanic rocks interactions. Notably, such interactions are capable of producing the extremely high concentration of H_2 measured in the Cl-depleted sample and thus the very unusual H_2/CH_4 observed [61] (Figure S4). High concentrations of metals are consistent with the highly acidic nature of the fluids coupled with high H_2/H_2S ratios [62, 63].

The relatively mild pH, $^3He/CO_2$, and R/Ra ratios of the Fatu Kapa fluids are diagnostic of the occurrence of seawater/MORB interactions [64–66] (Figure S5). Consistently, the geochemistry of the Fatu Kapa fluids was very similar to the Vienna Woods ones whose composition is mainly the result of interactions with basalts [3, 4]. Yet metal concentrations were lower at Fatu Kapa while Ca, K, and Rb were higher and Li is similar. Plausible explanations for the extremely low metal concentrations observed in the Fatu Kapa fluids are conductive cooling; water/metal-poor rocks interactions; subsurface metal trapping under silica and barite slabs [6]. Given the wide variety of lithologies sampled in the area, fluid compositions are likely the results of interactions with a wide range of rock source chemistries. To that respect, the composition of the local lavas that are characteristic of andesite, trachy-andesite, dacite, and trachy-dacite probably best explains the enrichment in Ca and in the mobile alkali metals K and Rb.

5.5. What Controls Organic Geochemistry? The origin of hydrocarbon gases and SVOCs in natural systems including hydrothermal systems has been the focus of many studies since the abiotic origin of some hydrocarbons was postulated ([67, 68] for a review). Both field and experimental studies have tried to unravel the origin of hydrocarbons making use of stable isotopes (e.g., reviews of [34, 35]). Although there are strong discrepancies among studies, the variation of $\delta^{13}C$ with the carbon number may be a reasonable indicator of the origin. The trend observed in the Cl-depleted sample of Kulo Lasi was very similar to the ones attributed to an abiogenic origin in the Precambrian shields or in the Lost City hydrothermal field [69, 70]. The Kulo Lasi Cl-rich sample exhibited a pattern that has been observed in several Fischer-Tropsch type (FTT) experiments [34]. The strong positive or negative fractionation between C_1 and C_2 observed in the hot fluids of Kulo Lasi is likely due to chain initiation [71]. Conversely, the low-T (135°C) sample that was collected in a beehive-type smoker covered with bacterial mats showed a regular positive trend which has been proposed to be diagnostic of a thermogenic origin. Although we concede that the abiogenic origin of C_{2+} hydrocarbon gases in the Kulo Lasi field will need more investigation, methane is clearly at the border of abiogenic and thermogenic domains both at Kulo Lasi and at Fatu Kapa with $\delta^{13}C$ values ranging from −29 to −6.1‰ ([72] and Figure 7). Carbon isotopes of CH_4 and CO_2 suggest that methane underwent oxidation, possibly by bacteria, at both sites and may explain the extremely low concentrations observed (Figure 8 in [73]). Consistently and according to thermodynamic calculations, methanogenesis should be limited under the P, T, and redox conditions present at the Futuna sites and CH_4 consumption might be prevalent [31].

By contrast, carbon isotopes have not appeared to be useful up to date in determining the origin of heavier organic compounds [74]. Several processes are likely to occur simultaneously and to use several C sources, resulting in a nondiagnostic bulk $\delta^{13}C$ signature. Several experimental and theoretical studies indicate that a range of organic compounds including linear alkanes and FAs could form and persist in natural hydrothermal systems (e.g., [31–35]). However, according to the calculated fH_2 at P and T of the study sites, the redox conditions are likely buffered by Hematite-Magnetite (HM) or an even more oxidizing mineral assemblage which appear less favourable for abiotic synthesis than Pyrite-Pyrrhotite-Magnetite, Fayalite-Magnetite-Quartz, or ultramafic rocks assemblages [27, 32, 33] (Table 4). The occurrence of organic compounds in our fluids must thus be attributed to a great part to other processes. Microbial production and thermal degradation of microorganisms, OM detritus, and/or refractory dissolved OM represent good candidates to produce soluble organic compounds. PAHs are indeed common products of pyrolysis of OM [26, 75, 76]. Long chained fatty acids are major constituent of organisms and their presence in the Futuna fluids could be easily associated with thermal degradation of biomass or OM [26, 77]. Yet the distribution of the compounds found in the fluids does not match a simple process of OM degradation. Only $>C_{13}$ n-FAs occurred in sediments with C_{16} being the most abundant (Figure S6). However, similar to our samples, both odd and even carbon number n-FAs were observed in the C_{14}–C_{20} range with odd FAs being less abundant. Petroleum exhibits nearly equal levels of C_{14}–C_{20} n-FAs. Only the even series has been reported in both massive sulphide deposits (MSD) and hydrothermal mussels with C_{16} being the most abundant. Short chain FAs ($<C_{13}$) have only been reported in Lost City fluids but here again only the even series occurred. In any case C_9 was reported whereas it was nearly the most abundant in our fluids. Abiotic processes may still be considered as nonanoic acid could be synthesized from CO_2

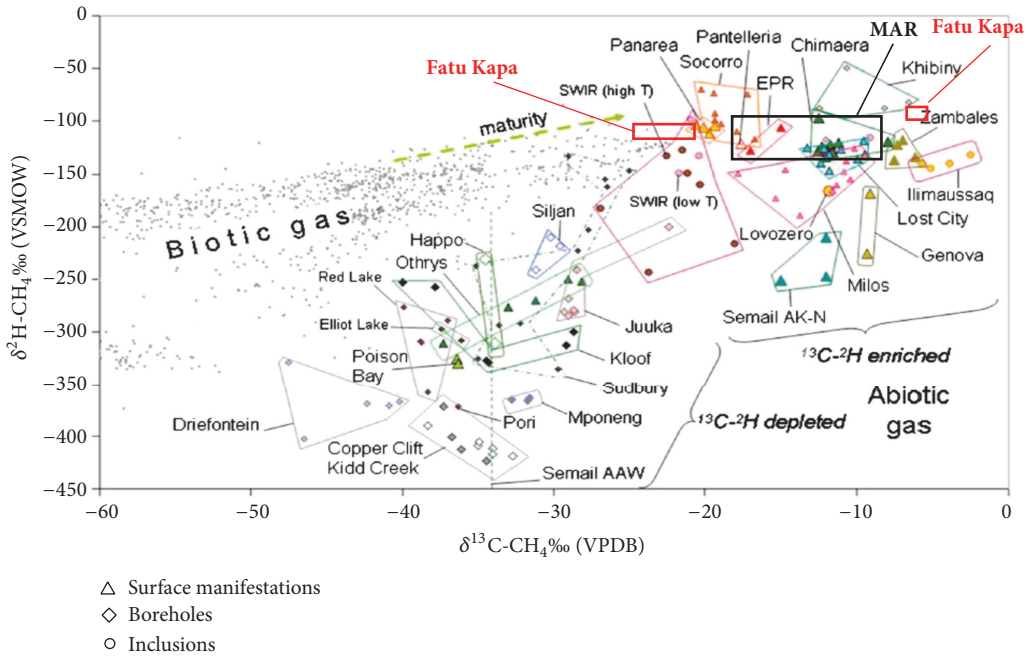

FIGURE 7: Modified after Etiope and Sherwood Lollar [9]. The isotopic composition of CH_4 in the Fatu Kapa fluids falls into the abiotic gas category but differs from the typical isotopic signature of CH_4 at Mid-Atlantic Ridge's vent fields.

and H_2 [31], nonane [78], or undecane [79]. As a difference the presence of C_{16} and C_{18} n-FAs in significant amount in the fluids from Fatu Kapa may represent a direct microbial contribution. The distribution observed in the Fatu Kapa fluids likely reflects the occurrence of several concomitant processes possibly including production reactions (abiotic and thermogenic) and consumption mechanisms (adsorption and complexation).

Nonvolatile n-alkanes are usually associated with lower *T* processes such as in oil fields or at the Middle Valley hydrothermal vent field [80]. In the Guaymas basin, where n-alkane-rich sediment samples have been reported, it is less clear what temperature they were exposed to. However and as far as we understood high temperatures were rather associated with absence of n-alkanes and presence of PAHs consistently with high-temperature OM pyrolysis [26, 81, 82]. Pyrolytic processes resulted in the presence of light hydrocarbon gases with an exception of some high *T* (>200°C) fluids containing C_9 and C_{10} n-alkanes. n-Alkanes also occur in solids from unsedimented hydrothermal vent fields ([76] and references therein). Notably, the n-alkanes distribution in our fluids does not resemble any aspects neither the ones resulting of low-*T* processes nor the ones created by high-*T* FTT reactions [83, 84] (Figure S7). C_{10}–C_{20} n-alkanes usually occur in equivalent amounts in petroleum or show a consistent decrease with molecular weight. Experimental FTT reactions produced consistent increasing concentrations from C_9 to C_{12} and then consistent decreasing concentrations to C_{20}. Similar patterns are also associated with the kerosene fraction of petroleum [85]. Distribution patterns in hydrothermal solids are difficult to picture as usually only chromatograms are provided in the studies, for example, [86], but they largely differ by the simple fact that $<C_{14}$ alkanes were not detected in most cases as in sediments from various locations [87]. The smaller alkanes may well be preferentially entrained in fluid circulation but they are more likely the result of other processes, especially high-temperature ones, and including abiotic reactions. Note that the latter should not be reduced to sole FTT reactions because supercritical water is a fabulous medium for unconventional reactions [88–90].

Formate and acetate have been given more attention in both laboratory [91–93] and field hydrothermal studies [28, 29] as these small molecules are likely to prevail according to thermodynamic studies (e.g., [31–33]). Where usually formate dominates, acetate was found to be more abundant in fluids from Fatu Kapa. According to Shock studies, at 280–300°C, formic acid concentrations should not be much higher than acetic acid, but this is not enough to explain our "reverse" concentrations. And especially it is not consistent with higher amounts in the 300°C fluids. A ratio close to 1 was observed at Kulo Lasi which may indicate that different production/consumption processes occur. Also the concentrations of the formate and acetate plotted on a line versus Mg which suggest that the fate of these volatile fatty acids at Kulo Lasi is controlled by simple mixing; that is there would be no consumption/production when fluid mixes with seawater (Figure 4). The deep-seawater concentrations were high compared to what is usually reported in the literature which was most likely due to plume contribution [27, 28]. This supports the simple mixing model hypothesis and is consistent with the near absence of organisms around those chimneys.

5.6. Organic Compounds: Implications for Biology, Mineral Resources, and C Cycling. The idea that life could have originated in hydrothermal systems from abiotic reactions was postulated in the late 70s [94]. However, the question of the origin of organic compounds in hydrothermal systems has remained ever since they were evidenced in natural environments [95]. On the one hand, a biogenic or thermogenic origin seems most likely for most compounds investigated so far; on the other hand, one cannot exclude that some of the formate and aliphatic hydrocarbons form abiotically [13, 26–28, 30, 96]. As detailed in the previous section, our results are consistent with a mix of origin although abiotic synthesis likely occurs to a far smaller extent than other processes that would overprint an abiotic signature.

Upon the hot topic of the origin of life, the mere presence of organic compounds is highly important for the fauna at the local and regional scales. It is well established that VFAs constitute a significant food source for some microorganisms and thus help sustaining hydrothermal ecosystems [97–100]. Besides, some bacteria have proven to be capable of using naphthalene [101] and tubeworms, hydrocarbons [102].

Organics can form complexes with metals [20, 21]. This greatly improves the dispersion of metals in the ocean and prevents them from precipitation as sulphides or oxyhydroxydes [23, 103]. Notably fatty acids are efficient ligands that play a major role in making metals bioavailable as well as in transporting them both through the upper crust ([17] and references therein) and through the water column in the plume [11, 104–106]. In addition, they have been shown to be involved in growth/dissolution processes of some minerals [19, 107]. For these reasons, they are of particular importance in ore-forming processes. Hydrocarbons which are weaker ligands would react with sulfates to generate bisulfide (HS^-), which in turn would easily react with metal chlorides to form metal sulphides according to the following mass balance equations:

$$3{SO_4}^{2-} + 3H^+ + 4R\text{–}CH_3 \longrightarrow 4R\text{–}CO_2H + HS^- + 4H_2O \quad (2)$$

$$HS^- + MeCl_2 \longrightarrow MeS + H^+ + 2Cl^- \quad (3)$$

where R is a carbonated chain, either aliphatic or aromatic, and represents OM [108]. To that respect hydrocarbons are likely to be involved in depositional processes of metals. Notably associations of aliphatic and aromatic hydrocarbons with mineral deposits have also been observed on the EPR [109] and in sulphide sedimentary deposits on land [104].

5.7. Fluxes: Importance of Back-Arc Hydrothermal Systems to the Ocean Geochemistry. Hydrothermal input to the ocean via plumes has long been neglected but recent results of the GEOTRACES program clearly show its importance in terms of metals and trace elements transportation and implications for ocean biogeochemistry [13, 110–113]. While it is now well established that MOR hydrothermal discharge has a large impact on the global ocean chemistry and element cycles, the relative impact of hydrothermal activity from other hydrothermal settings has not been established. The extensive hydrothermal activity reported in the Wallis and Futuna region suggests that back-arc system hydrothermalism may be of much greater importance than previously anticipated [7, 114]. Estimation of hydrothermal fluxes is generally challenging and very few data are available in the literature [115–118]. Therefore we believe that any kind of estimation, even orders of magnitudes are of importance to make advances in this field. We propose to combine two different approaches based on geophysical data and video recordings (see here), respectively, to propose such estimates with some confidence.

5.7.1. Estimation Using Geophysics. We can make an order of magnitude estimate of the heat flux from the different hydrothermally active areas based on the physical characteristics of the plumes. Marshall and coworkers [119–121] have proposed a scaling relationship between the heat flux at an interface, Hf, the ambient buoyancy frequency (N) in the surroundings of the plume, the characteristic size (R_s) of the heat transfer region, and the equilibrium height (or depth; h) reached by the plume, as

$$\mathrm{Hf} = \frac{(\rho \cdot Cp)}{(g \cdot \alpha \cdot R_s)} \cdot \left(N \cdot \frac{h}{5}\right)^3, \quad (4)$$

where ρ is seawater density (1030 kg·m^{-3}), Cp is heat capacity of seawater (~4000 J·kg^{-1}·K^{-1}), and g is gravitational acceleration (9.81 m·s^{-2}), and α is the thermal expansion coefficient of seawater (10^{-4} K^{-1}). The ambient buoyancy frequency (N) can be estimated to be between 0.001 and 0.002 s^{-1} from CTD profiles in the area using a routine in the UNESCO Sea Water Library described by Jackett and Mcdougall [122]. The radius (R_s) of the Kulo Lasi caldera is 2500 m and the plume rose in average about 200 m above seafloor (top layer boundary) [7]. For order of magnitude estimates, the ~130 km^2 Fatu Kapa area can be approximated by a disk of radius 6400 m, with a similar plume height. Introducing these numbers in (4) leads to heat flux estimates ranging between 100 and 800 W·m^{-2} for the Kulo Lasi caldera and 50 and 400 W·m^{-2} for the Fatu Kapa area, which is greatly dependent on the value for buoyancy frequency. While these estimates scale proportionally with the area considered to be hydrothermally active, they integrate the sources within the area which do not demand that the whole area be active. We estimate that total heat inputs are in the 2–16 GW for the Kulo Lasi caldera and 5–40 GW for the Fatu Kapa areas.

5.7.2. Estimation Based on Video Postprocessing. Video recordings could be used to estimate fluid velocities of the Carla and Obel^X chimneys and of a few smokers at Kulo Lasi using for instance the Typhoon algorithm [123] (Figures S8–S11). This optical flow method recovers the (2D) fluid flow from the apparent displacements, in an image sequence, of tracers advected by the flow. Here, the plume acts as the tracer. Compensation for the camera and vehicle motion and parallax correction were not possible, so the investigated video sequences where chosen according to (i) the overall stability of the camera and vehicle and (ii) the plume being as perpendicular to the camera as possible. The relevant

lengths scales (image spatial resolution and diameter of the chimneys) had to be estimated from known object sizes in the same ground, typically shrimps. External diameters of the chimney were used for calculation as any estimation of the internal diameter on video recordings would be too speculative. Note that (i) chimney samples taken at Kulo Lasi exhibited similar internal and external diameters; (ii) the large anhydrite chimneys (e.g., Obel^X, Carla) at Fatu Kapa did not seem to have any central conduit but rather exhibited a sponge-like structure leaking fluid at a high velocity from the entire volume. As a result, we believe the overestimation resulting from this assumption to be limited. Finally, the observed flow velocity is assumed to be constant across the jet section. Given all these limitations and assumptions, the resulting fluxes values should be taken as an indication of their order of magnitude.

The fluid velocity was estimated to be on average 0.05, 0.15, and 1 m s^{-1} for Kulo Lasi, Carla, and Obel^X, respectively. In terms of heat fluxes, Carla (diameter ca. 70 cm) would generate ~6 MW while Obel^X (diameter ca. 250 cm) would produce ~5.7 GW, respectively. Associated mass fluxes would be 54 L s^{-1} and 5 m^3 s^{-1} which means, for instance, that the single Obel^X chimney could generate an input of 2.6 $\times$ 10^7 mol y^{-1} CH_4 to the ocean. Comparatively, estimation of the total efflux of methane from serpentinisation ranges from 15 to 84 $\times$ 10^9 mol y^{-1} including 9 $\times$ 10^9 mol y^{-1} for the sole slow spreading ridges. Similarly, the Carla chimney would release about 5.7 $\times$ 10^3 mol y^{-1} of dodecane that may help forming 1.4 mol y^{-1} of metal sulphides (see Section 5.6). Cumulative observations during the dives brought to a total of 220 smokers of various sizes (~5 cm to ~2.5 m in diameter) and apparent flows (strong, medium, slow). We assigned the strong, medium, and slow flows observed to the velocities of Obel^X, Carla, and Kulo Lasi, respectively. At Kulo Lasi about 100 smokers were counted during the Nautile dives and all appeared very similar in diameter (~3 cm) and fluid flow (0.05). Keeping in mind these uncertainties, an order of magnitude of the heat and mass fluxes generated by hot smokers at Fatu Kapa are estimated to be 6.8 GW and 6 m^3 s^{-1} for the Fatu Kapa area versus 9 MW and 6 L s^{-1} for the Kulo Lasi caldera. This means, for example, that the total Fe flux from hot fluids emanating from the caldera would be up to 1.9 $\times$ 10^6 mol y^{-1} versus recent estimations of the global hydrothermal iron input that are about 10^9 mol y^{-1} [112, 124]. The average nonanoic acid concentration in Fatu Kapa purest fluids is 7.25 ppb, which would result in 1.4 $\times$ 10^6 mol y^{-1} released in the ocean by the Fatu Kapa hot smokers. The carboxylic acid functional group of fatty acids makes them good potential ligands to form coordination complexes with iron, which stabilises iron in the plume in its reduced form [103, 125]. Hence, the example of nonanoic acid suggests that fatty acids could largely contribute to iron stabilisation.

However, the high-temperature fluxes calculated above failed to include heat fluxes from diffusive venting, which was largely present in both areas and is thought to be an important part of the global hydrothermal heat flux (up to 98%) [126]. The surface of the diffusive areas was also assessed on the videos. However, because the velocity of diffusive fluids could not be estimated using Typhoon, we assumed hydrothermal waters are exiting the seafloor at the minimum velocity reported for low temperature flow (0.04 m s^{-1}) [127]. The cumulative surface of diffusive areas with a typical temperature of 10°C reached 100 m^2 at Kulo Lasi and 2885 m^2 at Fatu Kapa. In addition, a particular area of about 300 m^2 at Kulo Lasi consisted in hundreds of silica chimney diffusing a 40°C fluid [6]. The resulting contribution of diffuse venting to the heat flux would be 2.14 GW and 5.3 GW at Kulo Lasi and Fatu Kapa, respectively. This brings the total heat flux estimates at 2.15 GW and 12 GW, respectively, which is consistent with the estimates obtained using the lower N value as well as the fact that only a small portion of the total surface of the sites was explored with the submersible.

5.7.3. Summary. According to these different estimates heat efflux at Kulo Lasi and Fatu Kapa are conservatively estimated to be at least for 1-2 GW and 5–10 GW, respectively; this estimate is based on the low N value, whereas using the higher N suggests a flux almost 10x higher. It seems highly likely that the Wallis and Futuna active areas combined with the 3 calderas to the East [114] have a heat flux of >10 GW. Vent fields on MOR have been reported to generate between 10 MW and 25 GW ([116, 117, 127, 128] and references therein) and the total hydrothermal heat flux at MORs is estimated to be about 1000 GW [129, 130]. This suggests that the presently discovered area might be of significant importance in the global budget and that back-arc hydrothermal activity contributes as much as MOR systems, and, possibly more, to the global ocean chemistry and cycles. Few estimates of hydrothermal heat flux have been published and the relative importance of heat, fluid, and geochemical hydrothermal fluxes from different environments will require studies designed to more accurately gauge these fluxes.

6. Concluding Remarks

The study of the geochemical characteristics of hydrothermal fluids from the Wallis and Futuna area confirmed the great potential of the region to generate a variety of fluid chemistries, as it was expected considering its particular geological context. This supports the idea that the hydrothermal contribution of back-arc environments is of great interest for the global ocean chemistry. Our order of magnitude estimates of fluxes suggest that back-arc hydrothermal activity contributes as much as MOR systems and possibly more. Notably the sole Obel^X chimney could generate ~1‰ of the total hydrothermally derived CH_4. The diversity observed in the Wallis and Futuna area also emphasizes that each new field presents its own characteristics and that exploration should continue. A huge number of sites remain to be discovered according to the newly published estimation of vent fields occurring on Earth [131].

A special focus was brought on organic geochemistry because of the few data available in modern hydrothermal systems despite the recent growing interest for oceanic OM. Concentrations of SVOCs are the first to be reported which

will have implications in a wide range of questions and fields. Our results are relevant to the understanding of C cycling and complete the works by Hawkes and Rossel who demonstrated that DOM is recycled if not removed partially through hydrothermal systems but who could not identify compounds in DOM. Identification of organic molecules is especially needed to better understand organometallic chemistry at hydrothermal vents and thus utilisation by microbes, metal export, and ore-forming processes. The distribution patterns obtained revealed the occurrence of several processes controlling organic geochemistry and notably that one cannot exclude abiotic synthesis to occur in the study area but very likely to a so small extent that the signature would be overprinted.

This brings the idea that using natural concentrations to feed thermodynamic models of abiotic synthesis and/or guide the design of experimental work should enable making progress in unravelling the origin of organic compounds in hydrothermal systems. In addition, growing techniques as clumped isotopes [132] and position specific isotopes measurements [133] are available and should also help answering this question.

Conflicts of Interest

The authors declare that they have no conflicts of interest.

Acknowledgments

The 2010 and 2012 cruises to the French EEZ of Wallis and Futuna were financed through a public/private consortium of the French state, Ifremer, AAMP, and BRGM and industrial groups including Eramet, Technip, and Areva. The authors are very grateful to the ship crew and the ship captains JR. Glehen, P. Moimeaux, and R. Picard for running these three cruises with skills and professionalism. They acknowledge all the scientific parties of these cruises for their collaboration. They are also grateful to D. Pierre, C. Guerin, and A. Normand for processing bathymetric data on board and thank A.-S. Alix for providing the final maps. They are indebted to the physical oceanographers L. Marié and B. Le Cann who helped a lot with fluxes estimations and water mass physics. Finally, many thanks are due to P. Dérian from the Fluminance team (Inria, Rennes, France) who postprocessed video recordings using Thyphoon for fluxes estimation.

Supplementary Materials

Supplementary 1. S1: mixing lines used for calculation of the endmember composition of the Fatu Kapa fluids. S2: modified after Von Damm et al. [46]. Plot of the molality of dissolved SiO2 in equilibrium with quartz in seawater versus temperature for isobars from 1500 to 1000 bar according to Von Damm et al. model. The Si most enriched fluid collected at Kulo Lasi is represented by the blue star. The red circle covers the range of Si concentrations and T encountered in fluids from the Fatu Kapa vent field. S3: modified after Bischoff and Pitzer [53]. Stars stand for Kulo Lasi fluid phases characteristics. They nearly plot on the 150-bar isobar. The close-up of the 400°C, 300-bar region shows that seawater could produce the observed salinities at Kulo Lasi by phase separation at about 320–350 bar and 415–420°C. S4: modified after Kawagucci et al. [134]. Plots of H2 concentration versus CH4 concentration in various hydrothermal fluids. The grey area represents values observed in a hydrothermal experiment using natural seafloor sediments. Values obtained for the Wallis and Futuna vent fields are reported: Kulo Lasi brine and condensed vapour phases are marked by the red square and the blue diamond, respectively, and the blue shaded area covers the range of values obtained in the Fatu Kapa field. S5: modified after Lupton et al. [66]. (a) Plot summarizing 3He/4He ratio versus C/3He for various mantle provinces, including mid-ocean ridges (black-filled symbols), submarine arc volcanoes (blue), and sub aerial arc volcanoes (green). Values for the Fatu Kapa vent field are reported as orange diamonds. 3He/4He is expressed as R/Ra. Crosses indicate average values for MORBs and for subaerial arcs from. (b) Similar plot including values for hotspot volcanoes such as Loihi, Kilauea fumarole, Yellowstone Park gases, Reunion, and Fatu Kapa (orange diamonds). S6: distribution of linear fatty acids in various environments. Data are from [135] for Massive Sulphide Deposits (MSD); [36] for Lost City (LC) fluids; [136] for petroleum and recent and ancient sediments; [137] for 13°N mussels. S7: distribution of linear alkanes obtained by thermogenic maturation in various crude oil basins and abiotic Fischer-Tropsch type experiment [84]. S11: time series of the estimated displacements corresponding to the video sequences shown in Figures S8, S9, and S10.

Supplementary 2. S8: example of a postprocessed video sequence using the Typhoon algorithm to estimate displacements (instantaneous, left panel; averaged on 25 frames, right panel) on one of the small black smokers in the Kulo Lasi caldera.

Supplementary 3. S9: example of a postprocessed video sequence using the Typhoon algorithm to estimate displacements (instantaneous, left panel; averaged on 25 frames, right panel) at the base of the Carla chimney.

Supplementary 4. S10: example of a postprocessed video sequence using the Typhoon algorithm to estimate displacements (instantaneous, left panel; averaged on 25 frames, right panel) at the top of the massive Obel^{X} chimney. S11: time series of the estimated displacements corresponding to the video sequences shown in Figures S8, S9, and S10.

References

[1] S. E. Beaulieu, "InterRidge Global Database of Active Submarine Hydrothermal Vent Fields: prepared for InterRidge, Version 3.3," *World Wide Web electronic publication., Version 3.4*, 2015.

[2] Y. Fouquet, U. Vonstackelberg, J. L. Charlou et al., "Hydrothermal activity in the Lau back-arc basin:Sulfides and water chemistry," *Geology*, vol. 19, pp. 303–306, 1991.

[3] M. D. Hannington, C. D. J. de Ronde, and S. Petersen, "Sea-floor tectonics and submarine hydrothermal systems," in *Economic Geology 100th Anniversary Volume. Society of Economic Geologists*, J. W. Hedenquist, J. F. H. Thompson, R. J. Goldfarb, and

J. P. Richards, Eds., pp. 111–141, Society of Economic Geologists, Littelton, Colorado, USA, 2005.

[4] E. P. Reeves, J. S. Seewald, P. Saccocia et al., "Geochemistry of hydrothermal fluids from the PACMANUS, Northeast Pual and Vienna Woods hydrothermal fields, Manus Basin, Papua New Guinea," *Geochimica et Cosmochimica Acta*, vol. 75, no. 4, pp. 1088–1123, 2011.

[5] J. S. Seewald, E. P. Reeves, W. Bach et al., "Submarine venting of magmatic volatiles in the Eastern Manus Basin, Papua New Guinea," *Geochimica et Cosmochimica Acta*, vol. 163, pp. 178–199, 2015.

[6] Y. Fouquet, A. S. Alix, D. Birot et al., "Discovery of Extensive Hydrothermal Fields in the Wallis and Futuna Back-Arc Environment (SW Pacific)," in *Proceedings of the SGA - 13th Biennial Meeting - Mineral Resources in a Sustainable World*, SGA, Ed., pp. 1223–1226, Nancy, France, 2015.

[7] C. Konn, E. Fourré, P. Jean-Baptiste et al., "Extensive hydrothermal activity revealed by multi-tracer survey in the Wallis and Futuna region (SW Pacific)," *Deep-Sea Research Part I: Oceanographic Research Papers*, vol. 116, pp. 127–144, 2016.

[8] M. Bevis, F. W. Taylor, B. E. Schutz et al., "Geodetic observations of very rapid convergence and back-arc extension at the tonga arc," *Nature*, vol. 374, no. 6519, pp. 249–251, 1995.

[9] G. Etiope and B. Sherwood Lollar, "Abiotic methane on earth," *Reviews of Geophysics*, vol. 51, no. 2, pp. 276–299, 2013.

[10] R. M. W. Amon, "Carbon cycle: Ocean dissolved organics matter," *Nature Geoscience*, vol. 9, no. 12, pp. 864-865, 2016.

[11] S. A. Bennett, P. J. Statham, D. R. H. Green et al., "Dissolved and particulate organic carbon in hydrothermal plumes from the East Pacific Rise, 9∘50'N," *Deep-Sea Research Part I: Oceanographic Research Papers*, vol. 58, no. 9, pp. 922–931, 2011.

[12] J. A. Hawkes, C. T. Hansen, T. Goldhammer, W. Bach, and T. Dittmar, "Molecular alteration of marine dissolved organic matter under experimental hydrothermal conditions," *Geochimica et Cosmochimica Acta*, vol. 175, pp. 68–85, 2016.

[13] J. A. Hawkes, P. E. Rossel, A. Stubbins et al., "Efficient removal of recalcitrant deep-ocean dissolved organic matter during hydrothermal circulation," *Nature Geoscience*, vol. 8, no. 11, pp. 856–860, 2015.

[14] S. Q. Lang, D. A. Butterfield, M. D. Lilley, H. Paul Johnson, and J. I. Hedges, "Dissolved organic carbon in ridge-axis and ridge-flank hydrothermal systems," *Geochimica et Cosmochimica Acta*, vol. 70, no. 15, pp. 3830–3842, 2006.

[15] K. Longnecker, "Dissolved organic matter in newly formed sea ice and surface seawater," *Geochimica et Cosmochimica Acta*, vol. 171, pp. 39–49, 2015.

[16] J. A. Breier, B. M. Toner, S. C. Fakra et al., "Sulfur, sulfides, oxides and organic matter aggregated in submarine hydrothermal plumes at 9∘50'N East Pacific Rise," *Geochimica et Cosmochimica Acta*, vol. 88, pp. 216–236, 2012.

[17] J. Brugger, W. Liu, B. Etschmann, Y. Mei, D. M. Sherman, and D. Testemale, "A review of the coordination chemistry of hydrothermal systems, or do coordination changes make ore deposits?" *Chemical Geology*, vol. 447, pp. 219–253, 2016.

[18] J. N. Fitzsimmons, S. G. John, C. M. Marsay et al., "Iron persistence in a distal hydrothermal plume supported by dissolved-particulate exchange," *Nature Geoscience*, vol. 10, no. 3, pp. 195–201, 2017.

[19] Q. Gautier, U.-N. Berninger, J. Schott, and G. Jordan, "Influence of organic ligands on magnesite growth: A hydrothermal atomic force microscopy study," *Geochimica et Cosmochimica Acta*, vol. 155, pp. 68–85, 2015.

[20] L. J. A. Gerringa, M. J. A. Rijkenberg, V. Schoemann, P. Laan, and H. J. W. de Baar, "Organic complexation of iron in the West Atlantic Ocean," *Marine Chemistry*, vol. 177, pp. 434–446, 2015.

[21] J. A. Hawkes, D. P. Connelly, M. Gledhill, and E. P. Achterberg, "The stabilisation and transportation of dissolved iron from high temperature hydrothermal vent systems," *Earth and Planetary Science Letters*, vol. 375, pp. 280–290, 2013.

[22] W. B. Homoky, "Biogeochemistry: Deep ocean iron balance," *Nature Geoscience*, vol. 10, no. 3, pp. 162–164, 2017.

[23] S. G. Sander and A. Koschinsky, "Metal flux from hydrothermal vents increased by organic complexation," *Nature Geoscience*, vol. 4, no. 3, pp. 145–150, 2011.

[24] T. M. Seward, A. E. Williams-Jones, and A. A. Migdisov, "The Chemistry of Metal Transport and Deposition by Ore-Forming Hydrothermal Fluids A2," in *Treatise on Geochemistry*, H. D. Holland and K. K. Turekian, Eds., pp. 29–57, Elsevier, Oxford, England, 2nd edition, 2014.

[25] B. M. Toner, S. C. Fakra, S. J. Manganini et al., "Preservation of iron(II) by carbon-rich matrices in a hydrothermal plume," *Nature Geoscience*, vol. 2, no. 3, pp. 197–201, 2009.

[26] C. Konn, D. Testemale, J. Querellou, N. G. Holm, and J. L. Charlou, "New insight into the contributions of thermogenic processes and biogenic sources to the generation of organic compounds in hydrothermal fluids," *Geobiology*, vol. 9, no. 1, pp. 79–93, 2011.

[27] C. Konn, J. L. Charlou, J. P. Donval, N. G. Holm, F. Dehairs, and S. Bouillon, "Hydrocarbons and oxidized organic compounds in hydrothermal fluids from Rainbow and Lost City ultramafic-hosted vents," *Chemical Geology*, vol. 258, no. 3-4, pp. 299–314, 2009.

[28] S. Q. Lang, D. A. Butterfield, M. Schulte, D. S. Kelley, and M. D. Lilley, "Elevated concentrations of formate, acetate and dissolved organic carbon found at the Lost City hydrothermal field," *Geochimica et Cosmochimica Acta*, vol. 74, no. 3, pp. 941–952, 2010.

[29] J. M. McDermott, J. S. Seewald, C. R. German, and S. P. Sylva, "Pathways for abiotic organic synthesis at submarine hydrothermal fields," *Proceedings of the National Acadamy of Sciences of the United States of America*, vol. 112, no. 25, pp. 7668–7672, 2015.

[30] E. P. Reeves, J. M. McDermott, and J. S. Seewald, "The origin of methanethiol in midocean ridge hydrothermal fluids," *Proceedings of the National Acadamy of Sciences of the United States of America*, vol. 111, no. 15, pp. 5474–5479, 2014.

[31] E. Shock and P. Canovas, "The potential for abiotic organic synthesis and biosynthesis at seafloor hydrothermal systems," in *GEOFLUIDS*, pp. 161–192, Blackwell Publishing Ltd, Hoboken, New Jersey, USA, 2010.

[32] E. L. Shock, "Geochemical constraints on the origin of organic compounds in hydrothermal systems," *Origins of Life and Evolution of Biospheres*, vol. 20, no. 3-4, pp. 331–367, 1990.

[33] E. L. Shock, "Chapter 5 Chemical environments of submarine hydrothermal systems," *Origins of Life and Evolution of Biospheres*, vol. 22, no. 1-4, pp. 67–107, 1992.

[34] T. M. McCollom, "Laboratory simulations of abiotic hydrocarbon formation in earth's deep subsurface," *Reviews in Mineralogy and Geochemistry*, vol. 75, pp. 467–494, 2013.

[35] T. M. McCollom and J. S. Seewald, "Abiotic synthesis of organic compounds in deep-sea hydrothermal environments," *Chemical Reviews*, vol. 107, no. 2, pp. 382–401, 2007.

[36] T. M. McCollom, J. S. Seewald, and C. R. German, "Investigation of extractable organic compounds in deep-sea hydrothermal vent fluids along the Mid-Atlantic Ridge," *Geochimica et Cosmochimica Acta*, vol. 156, pp. 122–144, 2015.

[37] C. Konn, J.-L. Charlou, J.-P. Donval, and N. G. Holm, "Characterisation of dissolved organic compounds in hydrothermal fluids by stir bar sorptive extraction - gas chomatography - mass spectrometry. Case study: The Rainbow field (36◦N, Mid-Atlantic Ridge)," *Geochemical Transactions*, vol. 13, article no. 8, 2012.

[38] B. Pelletier, Y. Lagabrielle, M. Benoit et al., "Newly identified segments of the Pacific-Australia plate boundary along the North Fiji transform zone," *Earth and Planetary Science Letters*, vol. 193, no. 3-4, pp. 347–358, 2001.

[39] Y. Fouquet, E. Pelleter, C. Konn et al., "Volcanic and hydrothermal processes in submarine calderas: the Kulo Lasi example (SW Pacific," *Ore Geology Reviews*, 2017, In Revision.

[40] K. L. Von Damm, J. M. Edmond, B. Grant, C. I. Measures, B. Walden, and R. F. Weiss, "Chemistry of submarine hydrothermal solutions at 21 ◦N, East Pacific Rise," *Geochimica et Cosmochimica Acta*, vol. 49, no. 11, pp. 2197–2220, 1985.

[41] J.-L. Charlou and J.-P. Donval, "Hydrothermal methane venting between 12◦N and 26◦N along the Mid-Atlantic Ridge," *Journal of Geophysical Research: Atmospheres*, vol. 98, no. 6, pp. 9625–9642, 1993.

[42] K. Grasshoff, "A simultaneous multiple channel system for nutrient analysis in seawater with analog and digital data record," in *Advances in Automated Analysis*, pp. 135–145, Mediad Inc, New York, NY, USA, 1970.

[43] J. B. Mullin and J. P. Riley, "The colorimetric determination of silicate with special reference to sea and natural waters," *Analytica Chimica Acta*, vol. 12, no. C, pp. 162–176, 1955.

[44] E. Baltussen, P. Sandra, F. David, and C. Cramers, "Stir bar sorptive extraction (SBSE), a novel extraction technique for aqueous samples: theory and principles," *Journal of Microcolumn Separations*, vol. 11, no. 10, pp. 737–747, 1999.

[45] C. R. German and K. L. Von Damm, "Hydrothermal Processes," *Treatise on Geochemistry*, vol. 6-9, pp. 181–222, 2004.

[46] K. L. Von Damm, J. L. Bischoff, and R. J. Rosenbauer, "Quartz solubility in hydrothermal seawater: an experimental study and equation describing quartz solubility for up to 0.5 M NaCl solutions," *American Journal of Science*, vol. 291, no. 10, pp. 977–1007, 1991.

[47] J. L. Bischoff and R. J. Rosenbauer, "The critical point and two-phase boundary of seawater, 200-500◦C," *Earth and Planetary Science Letters*, vol. 68, no. 1, pp. 172–180, 1984.

[48] K. L. Von Damm, "Seafloor hydrothermal activity: black smoker chemistry and chimneys," *Annual Review of Earth & Planetary Sciences*, vol. 18, pp. 173–204, 1990.

[49] J. L. Bischoff and R. J. Rosenbauer, "Phase separation in seafloor geothermal systems; an experimental study of the effects on metal transport," *American Journal of Science*, vol. 287, no. 10, pp. 953–978, 1987.

[50] Y. Mei, D. M. Sherman, W. Liu, B. Etschmann, D. Testemale, and J. Brugger, "Zinc complexation in chloride-rich hydrothermal fluids (25-600◦C): A thermodynamic model derived from ab initio molecular dynamics," *Geochimica et Cosmochimica Acta*, vol. 150, pp. 265–284, 2015.

[51] N. J. Pester, K. Ding, and W. E. Seyfried, "Vapor-liquid partitioning of alkaline earth and transition metals in NaCl-dominated hydrothermal fluids: An experimental study from 360 to 465◦C, near-critical to halite saturated conditions," *Geochimica et Cosmochimica Acta*, vol. 168, pp. 111–132, 2015.

[52] M. Watanabe, T. Sato, H. Inomata et al., "Chemical reactions of C1 compounds in near-critical and supercritical water," *Chemical Reviews*, vol. 104, no. 12, pp. 5803–5821, 2004.

[53] J. L. Bischoff and K. S. Pitzer, "Liquid-vapor relations for the system NaCl-H2O: summary of the P-T- x surface from 300˚ to 500˚C," *American Journal of Science*, vol. 289, no. 3, pp. 217–248, 1989.

[54] D. I. Foustoukos and W. E. Seyfried Jr., "Quartz solubility in the two-phase and critical region of the NaCl-KCl-H2O system: Implications for submarine hydrothermal vent systems at 9◦50′N East Pacific Rise," *Geochimica et Cosmochimica Acta*, vol. 71, no. 1, pp. 186–201, 2007.

[55] S. D. Scott, "Chapter 16: Submarine hydrthermal systems and deposits," in *Geochemistry of Hydrothermal Ore Deposits*, H. L. Barnes, Ed., pp. 797–876, 3rd edition, 1997.

[56] M. J. Mottl, J. S. Seewald, C. G. Wheat et al., "Chemistry of hot springs along the Eastern Lau Spreading Center," *Geochimica et Cosmochimica Acta*, vol. 75, no. 4, pp. 1013–1038, 2011.

[57] T. Gamo, K. Okamura, J.-L. Charlou et al., "Acidic sulfate-rich hydrothermal fluids from the Manus back-arc basin, Papua New Guinea," *Geology*, vol. 25, no. 2, pp. 139–142, 1997.

[58] D. A. Butterfield, K.-I. Nakamura, B. Takano et al., "High SO2 flux, sulfur accumulation, and gas fractionation at an erupting submarine volcano," *Geology*, vol. 39, no. 9, pp. 803–806, 2011.

[59] C. E. J. de Ronde, G. J. Massoth, D. A. Butterfield et al., "Submarine hydrothermal activity and gold-rich mineralization at Brothers Volcano, Kermadec Arc, New Zealand," *Mineralium Deposita*, vol. 46, no. 5, pp. 541–584, 2011.

[60] C. E. J. de Ronde and V. K. Stucker, "Chapter 47 - Seafloor hydrothermal venting at volcanic arcs and backarcs A2," in *The Encyclopedia of Volcanoes*, Haraldur Sigurdsson, Ed., pp. 823–849, Academic Press, Amsterdam, Netherlands, 2nd edition, 2015.

[61] F. J. Sansone, J. A. Resing, G. W. Tribble, P. N. Sedwick, K. M. Kelly, and K. Hon, "Lava-seawater interactions at shallow-water submarine lava flows," *Geophysical Research Letters*, vol. 18, no. 9, pp. 1731–1734, 1991.

[62] M. J. Mottl, H. D. Holland, and R. F. Corr, "Chemical exchange during hydrothermal alteration of basalt by seawater-II. Experimental results for Fe, Mn, and sulfur species," *Geochimica et Cosmochimica Acta*, vol. 43, no. 6, pp. 869–884, 1979.

[63] W. E. Seyfried, N. Pester, and Q. Fu, "Phase Equilibria Controls on the Chemistry of Vent Fluids from Hydrothermal Systems on Slow Spreading Ridges: Reactivity Of Plagioclase and Olivine Solid Solutions and the pH-Silica Connection," *Diversity of Hydrothermal Systems on Slow Spreading Ocean Ridges*, pp. 297–320, 2013.

[64] P. Jean-Baptiste, J. L. Charlou, M. Stievenard, J. P. Donval, H. Bougault, and C. Mevel, "Helium and methane measurements in hydrothermal fluids from the mid-Atlantic ridge: The Snake Pit site at 23◦N," *Earth and Planetary Science Letters*, vol. 106, no. 1-4, pp. 17–28, 1991.

[65] P. Jean-Baptiste, E. Fourré, J.-L. Charlou, C. R. German, and J. Radford-Knoery, "Helium isotopes at the Rainbow hydrothermal site (Mid-Atlantic Ridge, 36◦14′N)," *Earth and Planetary Science Letters*, vol. 221, no. 1-4, pp. 325–335, 2004.

[66] J. Lupton, K. H. Rubin, R. Arculus et al., "Helium isotope, C/3He, and Ba-Nb-Ti signatures in the northern Lau Basin: Distinguishing arc, back-arc, and hotspot affinities," *Geochemistry, Geophysics, Geosystems*, vol. 16, no. 4, pp. 1133–1155, 2015.

[67] G. P. Glasby, "Abiogenic origin of hydrocarbons: An historical overview," *Resource Geology*, vol. 56, no. 1, pp. 83–96, 2006.

[68] V. G. Kutcherov and V. A. Krayushkin, "Deep-seated abiogenic origin of petroleum: From geological assessment to physical theory," *Reviews of Geophysics*, vol. 48, no. 1, Article ID RG1001, 2010.

[69] G. Proskurowski, M. D. Lilley, J. S. Seewald et al., "Abiogenic hydrocarbon production at lost city hydrothermal field," *Science*, vol. 319, no. 5863, pp. 604–607, 2008.

[70] B. Sherwood Lollar, T. D. Westgate, J. A. Ward, G. F. Slater, and G. Lacrampe-Couloume, "Abiogenic formation of alkanes in the earth's crust as a minor source for global hydrocarbon reservoirs," *Nature*, vol. 416, no. 6880, pp. 522–524, 2002.

[71] S. Sherwood Lollar, G. Lacrampe-Couloume, K. Voglesonger, T. C. Onstott, L. M. Pratt, and G. F. Slater, "Isotopic signatures of CH4 and higher hydrocarbon gases from Precambrian Shield sites: A model for abiogenic polymerization of hydrocarbons," *Geochimica et Cosmochimica Acta*, vol. 72, no. 19, pp. 4778–4795, 2008.

[72] G. Etiope, S. Vance, L. E. Christensen, J. M. Marques, and I. Ribeiro da Costa, "Methane in serpentinized ultramafic rocks in mainland Portugal," *Marine and Petroleum Geology*, vol. 45, pp. 12–16, 2013.

[73] M. J. Whiticar, "Carbon and hydrogen isotope systematics of bacterial formation and oxidation of methane," *Chemical Geology*, vol. 161, no. 1, pp. 291–314, 1999.

[74] C. Konn, J. L. Charlou, N. G. Holm, and O. Mousis, "The production of methane, hydrogen, and organic compounds in ultramafic-hosted hydrothermal vents of the mid-atlantic ridge," *Astrobiology*, vol. 15, no. 5, pp. 381–399, 2015.

[75] O. E. Kawka and B. R. T. Simoneit, "Polycyclic aromatic hydrocarbons in hydrothermal petroleums from the Guaymas Basin spreading center," *Applied Geochemistry*, vol. 5, no. 1-2, pp. 17–27, 1990.

[76] B. R. T. Simoneit, "Chapter 4 Aqueous organic geochemistry at high temperature/high pressure," *Origins of Life and Evolution of Biospheres*, vol. 22, no. 1-4, pp. 43–65, 1992.

[77] J. S. Seewald, W. E. Seyfried Jr., and E. C. Thornton, "Organic-rich sediment alteration: an experimental and theoretical study at elevated temperatures and pressures," *Applied Geochemistry*, vol. 5, no. 1-2, pp. 193–209, 1990.

[78] M. D. Schulte and E. L. Shock, "Aldehydes in hydrothermal solution: Standard partial molal thermodynamic properties and relative stabilities at high temperatures and pressures," *Geochimica et Cosmochimica Acta*, vol. 57, no. 16, pp. 3835–3846, 1993.

[79] J. S. Seewald, "Aqueous geochemistry of low molecular weight hydrocarbons at elevated temperatures and pressures: Constraints from mineral buffered laboratory experiments," *Geochimica et Cosmochimica Acta*, vol. 65, no. 10, pp. 1641–1664, 2001.

[80] B. R. T. Simoneit, W. D. Goodfellow, and J. M. Franklin, "Hydrothermal petroleum at the seafloor and organic matter alteration in sediments of Middle Valley, Northern Juan de Fuca Ridge," *Applied Geochemistry*, vol. 7, no. 3, pp. 257–264, 1992.

[81] O. E. Kawka and B. R. T. Simoneit, "Hydrothermal pyrolysis of organic matter in Guaymas Basin: I. Comparison of hydrocarbon distributions in subsurface sediments and seabed petroleums," *Organic Geochemistry*, vol. 22, no. 6, pp. 947–978, 1994.

[82] B. R. T. Simoneit, O. E. Kawka, and M. Brault, "Origin of gases and condensates in the Guaymas Basin hydrothermal system (Gulf of California)," *Chemical Geology*, vol. 71, no. 1-3, pp. 169–182, 1988.

[83] Y. V. Kissin, "Catagenesis and composition of petroleum: Origin of n-alkanes and isoalkanes in petroleum crudes," *Geochimica et Cosmochimica Acta*, vol. 51, no. 9, pp. 2445–2457, 1987.

[84] T. M. McCollom and J. S. Seewald, "Carbon isotope composition of organic compounds produced by abiotic synthesis under hydrothermal conditions," *Earth and Planetary Science Letters*, vol. 243, no. 1-2, pp. 74–84, 2006.

[85] S. C. Vishnoi, S. D. Bhagat, V. B. Kapoor, S. K. Chopra, and R. Krishna, "Simple gas chromatographic determination of the distribution of normal alkanes in the kerosene fraction of petroleum," *Analyst*, vol. 112, no. 1, pp. 49–52, 1987.

[86] B. R. T. Simoneit, "Petroleum generation in submarine hydrothermal systems: an update," *The Canadian Mineralogist*, vol. 26, pp. 827–840, 1988.

[87] J. B. Rapp, "A statistical approach to the interpretation of aliphatic hydrocarbon distributions in marine sediments," *Chemical Geology*, vol. 93, no. 1-2, pp. 163–177, 1991.

[88] N. Akiya and P. E. Savage, "Roles of water for chemical reactions in high-temperature water," *Chemical Reviews*, vol. 102, no. 8, pp. 2725–2750, 2002.

[89] S. Deguchi and K. Tsujii, "Supercritical water: A fascinating medium for soft matter," *Soft Matter*, vol. 3, no. 7, pp. 797–803, 2007.

[90] J. P. Ferris, "Chapter 6 Chemical markers of prebiotic chemistry in hydrothermal systems," *Origins of Life and Evolution of Biospheres*, vol. 22, no. 1-4, pp. 109–134, 1992.

[91] D. I. Foustoukos and J. C. Stern, "Oxidation pathways for formic acid under low temperature hydrothermal conditions: Implications for the chemical and isotopic evolution of organics on Mars," *Geochimica et Cosmochimica Acta*, vol. 76, pp. 14–28, 2012.

[92] T. M. McCollom and J. S. Seewald, "Experimental constraints on the hydrothermal reactivity of organic acids and acid anions: I. Formic acid and formate," *Geochimica et Cosmochimica Acta*, vol. 67, no. 19, pp. 3625–3644, 2003.

[93] T. M. McCollom and J. S. Seewald, "Experimental study of the hydrothermal reactivity of organic acids and acid anions: II. Acetic acid, acetate, and valeric acid," *Geochimica et Cosmochimica Acta*, vol. 67, no. 19, pp. 3645–3664, 2003.

[94] D. E. Ingmanson and M. J. Dowler, "Chemical evolution and the evolution of the Earth's crust," *Origins of Life*, vol. 8, no. 3, pp. 221–224, 1977.

[95] N. G. Holm and J. L. Charlou, "Initial indications of abiotic formation of hydrocarbons in the Rainbow ultramafic hydrothermal system, Mid-Atlantic Ridge," *Earth and Planetary Science Letters*, vol. 191, no. 1-2, pp. 1–8, 2001.

[96] P. E. Rossel, A. Stubbins, T. Rebling, A. Koschinsky, J. A. Hawkes, and T. Dittmar, "Thermally altered marine dissolved organic matter in hydrothermal fluids," *Organic Geochemistry*, vol. 110, pp. 73–86, 2017.

[97] J. G. Ferry, "The chemical biology of methanogenesis," *Planetary and Space Science*, vol. 58, no. 14-15, pp. 1775–1783, 2010.

[98] Y. J. Kim, H. S. Lee, E. S. Kim et al., "Formate-driven growth coupled with H2 production," *Nature*, vol. 467, no. 7313, pp. 352–355, 2010.

[99] S. Q. Lang, G. L. Früh-Green, S. M. Bernasconi et al., "Microbial utilization of abiogenic carbon and hydrogen in a serpentinite-hosted system," *Geochimica et Cosmochimica Acta*, vol. 92, pp. 82–99, 2012.

[100] T. Windman, N. Zolotova, F. Schwandner, and E. L. Shock, "Formate as an energy source for microbial metabolism in chemosynthetic zones of hydrothermal ecosystems," *Astrobiology*, vol. 7, no. 6, pp. 873–890, 2007.

[101] A. Galushko, D. Minz, B. Schink, and F. Widdel, "Anaerobic degradation of naphthalene by a pure culture of a novel type of marine sulphate-reducing bacterium," *Environmental Microbiology*, vol. 1, pp. 415–420, 1999.

[102] S. A. Bennett, C. V. Dover, J. A. Breier, and M. Coleman, "Effect of depth and vent fluid composition on the carbon sources at two neighboring deep-sea hydrothermal vent fields (Mid-Cayman Rise)," *Deep-Sea Research Part I: Oceanographic Research Papers*, vol. 104, pp. 122–133, 2015.

[103] S. A. Bennett, E. P. Achterberg, D. P. Connelly, P. J. Statham, G. R. Fones, and C. R. German, "The distribution and stabilisation of dissolved Fe in deep-sea hydrothermal plumes," *Earth and Planetary Science Letters*, vol. 270, no. 3-4, pp. 157–167, 2008.

[104] P. F. Greenwood, J. J. Brocks, K. Grice et al., "Organic geochemistry and mineralogy. I. Characterisation of organic matter associated with metal deposits," *Ore Geology Reviews*, vol. 50, pp. 1–27, 2013.

[105] W. Liu, D. C. McPhail, and J. Brugger, "An experimental study of copper(I)-chloride and copper(I)-acetate complexing in hydrothermal solutions between 50∘C and 250∘ and vapor-saturated pressure," *Geochimica et Cosmochimica Acta*, vol. 65, no. 17, pp. 2937–2948, 2001.

[106] D. A. Palmer and K. E. Hyde, "An experimental determination of ferrous chloride and acetate complexation in aqueous solutions to 300∘C," *Geochimica et Cosmochimica Acta*, vol. 57, no. 7, pp. 1393–1408, 1993.

[107] S. P. Franklin, A. Hajash Jr., T. A. Dewers, and T. T. Tieh, "The role of carboxylic acids in albite and quartz dissolution: An experimental study under diagenetic conditions," *Geochimica et Cosmochimica Acta*, vol. 58, no. 20, pp. 4259–4279, 1994.

[108] H. G. Machel, H. R. Krouse, and R. Sassen, "Products and distinguishing criteria of bacterial and thermochemical sulfate reduction," *Applied Geochemistry*, vol. 10, no. 4, pp. 373–389, 1995.

[109] B. R. T. Simoneit, M. Brault, and A. Saliot, "Hydrocarbons associated with hydrothermal minerals, vent waters and talus on the East Pacific Rise and Mid-Atlantic Ridge," *Applied Geochemistry*, vol. 5, no. 1-2, pp. 115–124, 1990.

[110] J. A. Resing, P. N. Sedwick, C. R. German et al., "Basin-scale transport of hydrothermal dissolved metals across the South Pacific Ocean," *Nature*, vol. 523, no. 7559, pp. 200–203, 2015.

[111] S. Roshan and J. Wu, "The distribution of dissolved copper in the tropical-subtropical north Atlantic across the GEOTRACES GA03 transect," *Marine Chemistry*, vol. 176, pp. 189–198, 2015.

[112] A. Tagliabue, L. Bopp, J.-C. Dutay et al., "Hydrothermal contribution to the oceanic dissolved iron inventory," *Nature Geoscience*, vol. 3, no. 4, pp. 252–256, 2010.

[113] J. Wu, S. Roshan, and G. Chen, "The distribution of dissolved manganese in the tropical-subtropical North Atlantic during US GEOTRACES 2010 and 2011 cruises," *Marine Chemistry*, vol. 166, pp. 9–24, 2014.

[114] J. E. Lupton, R. J. Arculus, J. Resing et al., "Hydrothermal activity in the Northwest Lau Backarc Basin: Evidence from water column measurements," *Geochemistry, Geophysics, Geosystems*, vol. 13, no. 1, Article ID Q0AF04, 2012.

[115] H. Elderfield and A. Schultz, "Mid-ocean ridge hydrothermal fluxes and the chemical composition of the ocean," *Annual Review of Earth and Planetary Sciences*, vol. 24, pp. 191–224, 1996.

[116] C. R. German, A. M. Thurnherr, J. Knoery, J.-L. Charlou, P. Jean-Baptiste, and H. N. Edmonds, "Heat, volume and chemical fluxes from submarine venting: A synthesis of results from the Rainbow hydrothermal field, 36∘N MAR," *Deep-Sea Research Part I: Oceanographic Research Papers*, vol. 57, no. 4, pp. 518–527, 2010.

[117] E. Mittelstaedt, J. Escartín, N. Gracias et al., "Quantifying diffuse and discrete venting at the Tour Eiffel vent site, Lucky Strike hydrothermal field," *Geochemistry, Geophysics, Geosystems*, vol. 13, no. 4, Article ID Q04008, 2012.

[118] J. Sarrazin, P. Rodier, M. K. Tivey, H. Singh, A. Schultz, and P. M. Sarradin, "A dual sensor device to estimate fluid flow velocity at diffuse hydrothermal vents," *Deep-Sea Research Part I: Oceanographic Research Papers*, vol. 56, no. 11, pp. 2065–2074, 2009.

[119] K. G. Speer and J. Marshall, "The growth of convective plumes at seafloor hot springs," *Journal of Marine Research*, vol. 53, no. 6, pp. 1025–1057, 1995.

[120] M. Visbeck, J. Marshall, and H. Jones, "Dynamics of isolated convective regions in the ocean," *Journal of Physical Oceanography*, vol. 26, no. 9, pp. 1721–1734, 1996.

[121] J. A. Whitehead, J. Marshall, and G. E. Hufford, "Localized convection in rotating stratified fluid," *Journal of Geophysical Research: Oceans*, vol. 101, no. 11, pp. 25705–25721, 1996.

[122] D. R. Jackett and T. J. Mcdougall, "Minimal Adjustment of Hydrographic Profiles to Achieve Static Stability," *Journal of Atmospheric and Oceanic Technology*, vol. 12, pp. 381–389, 1995.

[123] P. Dérian, C. F. Mauzey, and S. D. Mayor, "Wavelet-based optical flow for two-component wind field estimation from single aerosol lidar data," *Journal of Atmospheric and Oceanic Technology*, vol. 32, no. 10, pp. 1759–1778, 2015.

[124] G. Carazzo, A. M. Jellinek, and A. V. Turchyn, "The remarkable longevity of submarine plumes: Implications for the hydrothermal input of iron to the deep-ocean," *Earth and Planetary Science Letters*, vol. 382, pp. 66–76, 2013.

[125] I. Bauer and H.-J. Knölker, "Iron Complexes in Organic Chemistry," *Iron Catalysis in Organic Chemistry: Reactions and Applications*, pp. 1–27, 2008.

[126] E. T. Baker, G. J. Massoth, S. L. Walker, and R. W. Embley, "A method for quantitatively estimating diffuse and discrete hydrothermal discharge," *Earth and Planetary Science Letters*, vol. 118, no. 1-4, pp. 235–249, 1993.

[127] P. Ramondenc, L. N. Germanovich, K. L. Von Damm, and R. P. Lowell, "The first measurements of hydrothermal heat output at 9∘50′N, East Pacific Rise," *Earth and Planetary Science Letters*, vol. 245, no. 3-4, pp. 487–497, 2006.

[128] P. Jean-Baptiste, H. Bougault, A. Vangriesheim et al., "Mantle 3He in hydrothermal vents and plume of the Lucky Strike site (MAR 37∘17′N) and associated geothermal heat flux," *Earth and Planetary Science Letters*, vol. 157, no. 1-2, pp. 69–77, 1998.

[129] A. Schultz and H. Elderfield, "Controls on the physics and chemistry of seafloor hydrothermal circulation," *Philosophical Transactions of the Royal Society of London A: Mathematical, Physical and Engineering Sciences*, vol. 355, no. 1723, pp. 387–425, 1997.

[130] C. A. Stein and S. Stein, "Constraints on hydrothermal heat flux through the oceanic lithosphere from global heat flow," *Journal of Geophysical Research: Atmospheres*, vol. 99, no. 2, pp. 3081–3095, 1994.

[131] E. T. Baker, J. A. Resing, R. M. Haymon et al., "How many vent fields? New estimates of vent field populations on ocean ridges from precise mapping of hydrothermal discharge locations," *Earth and Planetary Science Letters*, vol. 449, pp. 186–196, 2016.

[132] D. A. Stolper, A. M. Martini, M. Clog et al., "Distinguishing and understanding thermogenic and biogenic sources of methane using multiply substituted isotopologues," *Geochimica et Cosmochimica Acta*, vol. 161, pp. 219–247, 2015.

[133] A. Gilbert, K. Yamada, K. Suda, Y. Ueno, and N. Yoshida, "Measurement of position-specific 13C isotopic composition of propane at the nanomole level," *Geochimica et Cosmochimica Acta*, vol. 177, pp. 205–216, 2016.

[134] S. Kawagucci, Y. Ueno, K. Takai et al., "Geochemical origin of hydrothermal fluid methane in sediment-associated fields and its relevance to the geographical distribution of whole hydrothermal circulation," *Chemical Geology*, vol. 339, pp. 213–225, 2013.

[135] M. Blumenberg, R. Seifert, S. Petersen, and W. Michaelis, "Biosignatures present in a hydrothermal massive sulfide from the Mid-Atlantic Ridge," *Geobiology*, vol. 5, no. 4, pp. 435–450, 2007.

[136] J. E. Cooper and E. E. Bray, "A postulated role of fatty acids in petroleum formation," *Geochimica et Cosmochimica Acta*, vol. 27, no. 11, pp. 1113–1127, 1963.

[137] F. Ben-Mlih, J.-C. Marty, and A. Fiala-Medioni, "Fatty acid composition in deep hydrothermal vent symbiotic bivalves," *Journal of Lipid Research*, vol. 33, no. 12, pp. 1797–1806, 1992.